Journal of Computational Physics 229 (2010) 3474–3501

Contents lists available at ScienceDirect

Journal of Computational Physics

journal homepage: www.elsevier.com/locate/jcp

Spatially adaptive stochastic numerical methods for intrinsic fluctuations in reaction–diffusion systems ☆

Paul J. Atzberger *

University of California, Department of Mathematics, Santa Barbara, CA 93106, United States

ARTICLE INFO

Article history:
Received 19 November 2008
Received in revised form 19 September 2009
Accepted 13 January 2010
Available online 21 January 2010

Keywords:
Adaptive methods
Stochastic numerical methods
Stochastic partial differential equations
Reaction–diffusion
Multilevel meshes
MAC discretization
Statistical physics
Fluctuation–dissipation principle
Pattern formation
Gray–Scott reactions
Gradient sensing

ABSTRACT

Stochastic partial differential equations are introduced for the continuum concentration fields of reaction–diffusion systems. The stochastic partial differential equations account for fluctuations arising from the finite number of molecules which diffusively migrate and react. Spatially adaptive stochastic numerical methods are developed for approximation of the stochastic partial differential equations. The methods allow for adaptive meshes with multiple levels of resolution, Neumann and Dirichlet boundary conditions, and domains having geometries with curved boundaries. A key issue addressed by the methods is the formulation of consistent discretizations for the stochastic driving fields at coarse-refined interfaces of the mesh and at boundaries. Methods are also introduced for the efficient generation of the required stochastic driving fields on such meshes. As a demonstration of the methods, investigations are made of the role of fluctuations in a biological model for microorganism direction sensing based on concentration gradients. Also investigated, a mechanism for spatial pattern formation induced by fluctuations. The discretization approaches introduced for SPDEs have the potential to be widely applicable in the development of numerical methods for the study of spatially extended stochastic systems.

1. Introduction

In many systems a fundamental role is played by the spatial distribution of molecular species which undergo diffusive migrations while participating in chemical reactions. Examples include the synthesis and processing of materials, intracellular signaling in biology, and morphogenic processes in the development of tissues [38,49–53,70,73]. In many reaction–diffusion systems, the most interesting features are exhibited only in a sub-region of the spatial domain, such as in a chemically active front or in a layer near boundaries. Also, in many systems, an important role is played by the conditions at the boundaries or by the geometry of the boundaries [33,51,52]. A commonly used approach to model such reaction–diffusion systems is to use continuum field descriptions at the mean-field level for the local concentration of a molecular species. Such models are often expressed in terms of deterministic partial differential equations (PDEs). While this approach works well for many problems, at sufficiently small length-scales fluctuations are expected to arise in continuum field descriptions as a consequence of the finite number of molecules and neglected microscopic positional and momenta degrees of freedom.

☆ Work supported by NSF Grant DMS-0635535.
* Tel.: +1 805 893 3239.
E-mail address: atzberg@math.ucsb.edu.

0021-9991/$ - see front matter © 2010 Elsevier Inc. All rights reserved.
doi:10.1016/j.jcp.2010.01.012

To account for such fluctuations, we formulate stochastic partial differential equations (SPDEs) which introduce Gaussian stochastic fields into the PDE description of reaction–diffusion systems. We consider contributions from the intrinsic density fluctuations arising primarily from the finite number of molecules undergoing diffusive migrations, as opposed to fluctuations arising from the chemical reactions. The fluctuations are modeled by the stochastic fields using the fluctuation–dissipation principle of statistical mechanics.

When numerically approximating SPDEs, a number of issues arise which are not present in the corresponding deterministic setting. Numerical approximation of SPDEs requires both discretization of the partial differential equations and discretization of the stochastic driving fields. As a consequence of the stochastic driving fields, solutions of SPDEs are often not as smooth as solutions of the corresponding undriven deterministic PDE. Solutions of SPDEs often exist only in a generalized sense in a space of non-differentiable functions or in a space of linear functionals (distributions) [45,47,48,54]. Caution must be taken when formulating discretizations for such solutions. For example, traditional approaches such as finite difference methods often rely on the Taylor Theorem which requires smoothness to ensure accuracy. As an alternative, spectral methods can be formulated for SPDEs which rely on less-stringent results from approximation theory to ensure accuracy [24,25]. Fourier series provide one widely used approach for spectral approximation. While such spectral methods are useful for many SPDEs, they are typically restricted to domains having periodic boundaries or rather simple geometries and are often not readily amenable to adaptivity. To cope with this issue, finite element methods have also been introduced for the approximation of SPDEs [26]. As a consequence of the non-smoothness of solutions the rate of convergence is much slower than in the deterministic setting [26,27].

We shall introduce an approach for the derivation of discretizations based on finite difference methods for the approximation of SPDEs. To obtain accurate methods, the approach approximates solutions of the SPDEs by stochastic field values which correspond to solutions which are spatially averaged on length-scales comparable to the lattice spacing of the discretization mesh. Stochastic numerical methods are formulated allowing for adaptive multilevel meshes, Neumann and Dirichlet boundary conditions, and domains having geometries with curved boundaries. A key issue addressed by the methods is the development of consistent discretizations of the stochastic driving fields at coarse-refined interfaces of the mesh and at boundaries. As a demonstration of the issues encountered at coarse-refined interfaces, an empirical study is performed to show results for different discretization choices at such interfaces. For the derived discretizations, analysis is carried out which shows convergence of the methods as the underlying mesh is refined.

As a demonstration of the developed stochastic numerical methods, simulation studies are carried out for two applications. The first application studies the effect of fluctuations in microorganism direction sensing based on concentration gradients. The case investigated concerns a single cell which senses concentration gradients in an environment exhibiting a shallow gradient obscured by fluctuations. The biological cell is represented by a region having a disk-like geometry with Neumann boundary conditions. A gradient is induced in the concentration of an external signaling molecule by specifying at two walls the concentrations through Dirichlet boundary conditions. The stochastic numerical methods are utilized on a domain having a geometry defined by the two walls and region exterior to the disk. Results are reported for the role of fluctuations in a biological model recently proposed for cell gradient sensing [33].

The second application studies fluctuation-induced pattern formation in spatially extended systems. A variant of the Gray–Scott chemical reactions is considered in a regime where the deterministic reaction–diffusion system only exhibits a localized stationary pattern. When introducing fluctuations, a rich collection of patterns emerge over time, in which spotted patterns migrate, combine, and replicate. The adaptive features of the stochastic numerical methods are used to track at high resolution the dynamically evolving regions where the reactions are chemically active.

The proposed SPDEs give a model for intrinsic concentration fluctuations in reaction–diffusion systems. At the level of the continuum concentration fields, the model captures fluctuations arising from the finite number of molecules undergoing diffusive migrations. The stochastic numerical methods allow for adaptive approximation of solutions on domains having rather general geometries and boundary conditions. The approaches introduced for the derivation of discretizations for the SPDEs and for the development of the numerical methods are expected to be widely applicable in the study of spatially extended stochastic systems.

2. SPDEs accounting for fluctuations in reaction–diffusion systems

Reaction–diffusion systems are often modeled by partial differential equations which account for the evolution of the continuum concentration fields as the molecular species diffusively migrate and undergo chemical reactions. At sufficiently small length-scales, fluctuations arise in continuum field descriptions as a consequence of the finite number of molecules and as a consequence of neglected microscopic positional and momenta degrees of freedom. To account for such fluctuations in reaction–diffusion systems we consider stochastic partial differential equations (SPDEs) of the form

$$\frac{\partial \mathbf{c}(\mathbf{x},t)}{\partial t} = \nabla_{\mathbf{x}} \cdot \mathbf{D}\nabla_{\mathbf{x}}\mathbf{c}(\mathbf{x},t) + \mathbf{F}[\mathbf{c}] + \mathbf{n}(\mathbf{x},t), \tag{2.1}$$

$$\langle \mathbf{n}(\mathbf{x},t)\mathbf{n}^T(\mathbf{x}',t)\rangle = \mathbf{\Lambda}(\mathbf{x},\mathbf{x}')\delta(t-t'). \tag{2.2}$$

In the notation, $\mathbf{c}$ denotes the composite vector of concentration fields for the chemical species. The term $\nabla_{\mathbf{x}} \cdot \mathbf{D}\nabla_{\mathbf{x}}\mathbf{c}$ accounts for diffusion of the chemical species and is based on a generalization of Fick's Law allowing for non-isotropic diffusion. The

tensor $\mathbf{D}$ characterizes the rate at which chemical species undergo diffusive migrations and is assumed to be symmetric and positive definite. Throughout, we assume that the chemical species diffuse independently, which corresponds to $\mathbf{D}$ being a matrix which is block diagonal. The block matrices $\mathbf{D}^{(i)}$ correspond to the diffusion of the ith chemical species and are of size $d \times d$, where d is the number of spatial dimensions. The term $\mathbf{F}$ accounts for the chemical reactions. In general, $\mathbf{F}$ denotes a non-linear functional of the concentration fields which can be either stochastic or deterministic. In the present work, we consider only the case where $\mathbf{F}$ depends deterministically on $\mathbf{c}$. Throughout, $\mathbf{F}$ will be treated generically with only specific forms for the functional defined in Sections 9.1, 9.2 and 9.3. The term $\mathbf{n}$ accounts for fluctuations and is a Gaussian stochastic field which is δ-correlated in time with mean zero and spatial covariance $\mathbf{\Lambda}$. In the notation, $\langle\cdot\rangle$ denotes expectation with respect to the probability distribution of a random variable.

To derive a specific form for the Gaussian stochastic field $\mathbf{n}$ we make a number of simplifying assumptions. We consider the physical regime where fluctuations are small relative to the mean concentration. We also consider the case where fluctuations are dominated by contributions from the diffusive migrations of the molecular species as opposed to the chemical reactions. These assumptions correspond to the fluctuations of the concentration field at thermodynamic equilibrium having covariance [4,5,7–9]

$$\langle (c(\mathbf{x}) - \bar{c})(c(\mathbf{x}') - \bar{c})\rangle = \bar{c}\delta(\mathbf{x} - \mathbf{x}'), \tag{2.3}$$

where $\bar{c}$ denotes the mean concentration. To determine the spatial covariance structure of $\mathbf{n}$ we use a variant of the fluctuation–dissipation principle of statistical mechanics.

At thermodynamic equilibrium and within the regime of linear responses of the system, the fluctuation–dissipation principle maintains that relaxation from a perturbed state caused by an external field occurs in the same manner as relaxation from a perturbed state caused by fluctuations [2,7]. As a consequence, the dissipative operators of the dynamics and equilibrium covariance can be related to the covariance structure of the fluctuations driving the system. This can be expressed as, see [2,7],

$$\mathbf{\Lambda} = -\mathbf{AC} - \mathbf{C}^*\mathbf{A}^*, \tag{2.4}$$

where $\mathbf{A}^*$, $\mathbf{C}^*$ denote the adjoint of the operators. From Eqs. (2.2) and (2.3) we have

$$\mathbf{A} = \nabla_{\mathbf{x}} \cdot \mathbf{D}\nabla_{\mathbf{x}}, \tag{2.5}$$

$$\mathbf{C} = \bar{\mathbf{c}}\delta(\mathbf{x} - \mathbf{x}'). \tag{2.6}$$

Since the product of the operators in this case is self-adjoint the covariance structure of the driving fluctuations can be expressed as

$$\mathbf{\Lambda}_{ij}(\mathbf{x}, \mathbf{x}') = -2\bar{c}_i\delta_{ij}\nabla_{\mathbf{x}} \cdot \mathbf{D}^{(i)}\nabla_{\mathbf{x}}\delta(\mathbf{x} - \mathbf{x}'), \tag{2.7}$$

where for the ith molecular species $\bar{c}_i = \langle c_i\rangle$ denotes the mean concentration. We have used that $\mathbf{AC} = (\mathbf{AC})^* = \mathbf{C}^*\mathbf{A}^*, \mathbf{\Lambda} = -2\mathbf{AC}$. This determines the stochastic driving field $\mathbf{n}$ in Eq. (2.2) since $\mathbf{n}$ is Gaussian. The stochastic partial differential equations provide a model at the continuum level for the near equilibrium fluctuations in the concentration fields of reaction–diffusion systems.

3. Discrete approximation of the SPDEs

For SPDEs, numerical approximation requires both discretization of the partial differential equations and discretization of the stochastic driving fields. When numerically approximating SPDEs of the form of Eq. (2.2), issues arise which are not present in the corresponding deterministic PDE setting. As a consequence of the stochastic driving fields, solutions are not defined pointwise but only in a generalized sense in a space of linear functionals (distributions) [45,47,48,54]. We formulate discretizations which approximate numerically the action of these linear functionals.

For discretization in space of Eq. (2.2) and the stochastic driving field $\mathbf{n}$, we divide the spatial domain Ω into a partition of cells $\{\Omega_{\mathbf{m}}\}_{\mathbf{m}=1}^{M}$. The partition is required to have the property $\Omega = \cup_{\mathbf{m}=1}^{M}\Omega_{\mathbf{m}}$. The partition is also required to have intersections which are of measure zero $\nu(\Omega_\ell \cap \Omega_{\mathbf{m}}) = 0$, for $\ell \neq \mathbf{m}$, under the Lebesgue measure ν [42]. To approximate solutions numerically, we use stochastic field values obtained by averaging solutions over the volume of each partition cell

$$\mathbf{c}_{\mathbf{m}}(t) = \frac{1}{|\Omega_{\mathbf{m}}|}\int_{\Omega_{\mathbf{m}}} \mathbf{c}(\mathbf{x}, t)d\mathbf{x}. \tag{3.1}$$

To approximate the dynamics of $\mathbf{c}_{\mathbf{m}}(t)$, we use a stochastic process satisfying

$$d\mathbf{c}_t = L\mathbf{c}_t dt + \mathbf{f}dt + d\mathbf{g}_t. \tag{3.2}$$

In the notation, $\mathbf{c}_t$ denotes the composite vector of concentrations over all chemical species and all the sets $\Omega_{\mathbf{m}}$ at time t. The term L is a discrete operator which accounts for diffusion of the molecular species and approximates $\nabla \cdot \mathbf{D}\nabla$ in Eq. (2.2). The term $\mathbf{f}$ accounts for the chemical reactions and approximates $\mathbf{F}$. The term $\mathbf{g}_t$ is an Ito stochastic process accounting for fluctuations and approximates $\mathbf{n}$ [8,11]. The Eq. (3.2) is to be interpreted in the sense of an Ito Stochastic Differential Equation [8,11].

The stochastic driving field $\mathbf{n}$ of the continuum system given in Eq. (2.1) is a Gaussian process with mean zero and with δ-correlation in time. Since the averaging procedure of Eq. (3.1) is linear, we also take $\mathbf{g}_t$ to be a Gaussian stochastic process with mean zero and with δ-correlation in time. With this assumption the process $\mathbf{g}_t$ can be expressed in terms of increments of Brownian motion as

$$d\mathbf{g}_t = Qd\mathbf{B}_t. \tag{3.3}$$

In the notation, $d\mathbf{B}_t$ are increments of a vector-valued Brownian motion with n independent components and Q is an $m \times n$ matrix [11]. A particularly useful property of expression (3.3) is that Q can be directly related to the spatial covariance Γ of the stochastic process $\mathbf{g}_t$ by

$$\langle d\mathbf{g}_t d\mathbf{g}_{t'}^T \rangle = \langle Qd\mathbf{B}_t d\mathbf{B}_{t'}^T Q^T \rangle = QI\delta(t-t')dtdt'Q^T = \Gamma\delta(t-t')dtdt'. \tag{3.4}$$

This implies that

$$\Gamma = QQ^T. \tag{3.5}$$

We have used the identity of Ito Calculus that $\langle d\mathbf{B}_t d\mathbf{B}_{t'}^T \rangle = I\delta(t-t')dtdt'$, which in our notation corresponds to Ito's Isometry [11].

In this approach to approximating SPDEs, the discretization of the partial differential equation and the stochastic driving field play an inter-connected role in the equilibrium fluctuations exhibited by the discretized system. A consistent choice for these two components of the discretization is required to ensure that the discretized system accurately approximates the equilibrium fluctuations of the continuum system. We let the covariance of the equilibrium fluctuations of the discrete system be denoted by

$$C = \langle (\mathbf{c} - \bar{\mathbf{c}})(\mathbf{c} - \bar{\mathbf{c}})^T \rangle. \tag{3.6}$$

Since the stochastic fields are Gaussian, this requires the covariance matrix C approximate the covariance operator $\mathbf{C}$ of Eq. (2.6). We study specific forms taken by C in later sections.

We now derive a variant of the fluctuation–dissipation principle of statistical mechanics for the discretized system which establishes a relationship between L, C, and Γ. This is carried out in the case when $\mathbf{F} = 0$. For this purpose we consider at time t the covariance of concentration fluctuations

$$C_t = \langle (\mathbf{c}_t - \bar{\mathbf{c}})(\mathbf{c}_t - \bar{\mathbf{c}})^T \rangle. \tag{3.7}$$

From Ito's Lemma [11] and Eq. (3.2) we have

$$\begin{aligned} d[(\mathbf{c}_t - \bar{\mathbf{c}})(\mathbf{c}_t - \bar{\mathbf{c}})^T] &= (d\mathbf{c}_t)(\mathbf{c}_t - \bar{\mathbf{c}})^T + (\mathbf{c}_t - \bar{\mathbf{c}})(d\mathbf{c}_t)^T + (d\mathbf{c}_t)(d\mathbf{c}_t)^T \\ &= L(\mathbf{c}_t - \bar{\mathbf{c}})(\mathbf{c}_t - \bar{\mathbf{c}})^T dt + (\mathbf{c}_t - \bar{\mathbf{c}})(\mathbf{c}_t - \bar{\mathbf{c}})^T L^T dt + QQ^T dt + Qd\mathbf{B}_t(\mathbf{c}_t - \bar{\mathbf{c}})^T + (\mathbf{c}_t - \bar{\mathbf{c}})d\mathbf{B}_t^T Q^T. \end{aligned} \tag{3.8}$$

In our notation, Ito's Lemma [11] corresponds to $d\mathbf{B}_t d\mathbf{B}_t^T = Idt, dtdt = 0$, and $d\mathbf{B}_t dt = dtd\mathbf{B}_t^T = 0$. Taking the expectation in probability of both sides of Eq. (3.8) we obtain

$$dC_t = (LC_t + C_t L^T + \Gamma)dt. \tag{3.9}$$

This was obtained by using $\Gamma = QQ^T$, $\langle d\mathbf{B}_t \rangle = 0$, and Eq. (3.7).

As the system approaches the statistical steady-state, corresponding to thermodynamic equilibrium, we have $C_t \to C$ and $dC_t \to 0$. From Eq. (3.9) this yields

$$\Gamma = -\left(LC + CL^T\right). \tag{3.10}$$

In the case that LC is symmetric, this expression simplifies to

$$\Gamma = -2LC. \tag{3.11}$$

This establishes a fluctuation–dissipation principle for the discretized system relating L, C, and Γ.

To obtain consistent discretizations of both the partial differential equation and stochastic driving field, we use Eq. (3.10) to determine a Γ so that the error is controlled in the discrete system when approximating the equilibrium fluctuations of the continuum system. For this purpose, we require the discrete system have equilibrium fluctuations with covariance

$$C_{\ell,\mathbf{m}} = \left\langle (\mathbf{c}_\ell - \bar{\mathbf{c}}_\ell)(\mathbf{c}_\mathbf{m} - \bar{\mathbf{c}}_\mathbf{m})^T \right\rangle = \frac{\overline{C}}{|\Omega_\mathbf{m}|}\delta_{\ell,\mathbf{m}}. \tag{3.12}$$

The $\overline{C}_{ij} = \bar{c}_i\delta_{ij}$ and $\bar{c}_i = \langle c_i \rangle$. This determines Γ from Eq. (3.10). This choice for C corresponds to the equilibrium fluctuations of the continuum system spatially averaged over each partition cell $\Omega_\mathbf{m}$. For any choice of partition $\Omega_\mathbf{m}$ and consistent discretization L, Eq. (3.10) gives a covariance structure Γ for the stochastic driving field which realizes a given choice of C for the equilibrium fluctuations. Formally, as the mesh is refined, if we have $C \to \mathbf{C}$ and $L \to \mathbf{A} = \nabla_\mathbf{x} \cdot \mathbf{D}\nabla_\mathbf{x}$, then we have $\Gamma = -LC - CL^T \to -\mathbf{AC} - \mathbf{C}^*\mathbf{A}^* = \mathbf{\Lambda}$. This suggests that such an approach provides a means to obtain consistent discretizations

of the stochastic driving field $\mathbf{n}$ of Eq. (2.2), while controlling the errors in the equilibrium fluctuations of the discrete system. After deriving specific discretizations using this approach and developing stochastic numerical methods to generate efficiently the required stochastic fields, we revisit the issue of convergence in Section 8.

4. Transformation of the operator $\nabla \cdot D\nabla$ to the Laplacian

A change of variable can be made which transformations $\nabla \cdot \mathbf{D}\nabla$ into a standard Laplacian Δ. This will be used to put the differential operator into a more convenient form for numerical approximation. The change of variable is based on the special properties of $\mathbf{D}$.

Since the chemical species are assumed to diffuse independently, the diffusion tensor $\mathbf{D}$ has diagonal blocks $\mathbf{D}^{(k)}$ of size $d \times d$, where d is the spatial dimension of the system. This allows for the full differential operator to be decomposed into a sum of components of the form

$$\nabla_{\mathbf{x}} \cdot \mathbf{D}\nabla_{\mathbf{x}} = \sum_k \nabla_{\mathbf{x}} \cdot \mathbf{D}^{(k)} \nabla_{\mathbf{x}}. \tag{4.1}$$

The block matrix $\mathbf{D}^{(k)}$ corresponds to diffusion of the kth chemical species. Each matrix $\mathbf{D}^{(k)}$ is symmetric and can be diagonalized by a unitary matrix

$$\tilde{\mathbf{D}}^{(k)} = (P^{(k)})^T \mathbf{D}^{(k)} P^{(k)}, \tag{4.2}$$

where $\tilde{\mathbf{D}}^{(k)}$ denotes a diagonal matrix and $P^{(k)}$ denotes a unitary matrix. Under the linear change of variable $\tilde{\mathbf{x}} = R\mathbf{x}$, the gradient and divergence operators become

$$\nabla_{\mathbf{x}} = R\nabla_{\tilde{\mathbf{x}}}, \tag{4.3}$$

$$\nabla_{\mathbf{x}} \cdot = \nabla_{\tilde{\mathbf{x}}} \cdot R^T. \tag{4.4}$$

This gives

$$\nabla_{\mathbf{x}} \cdot \mathbf{D}^{(k)} \nabla_{\mathbf{x}} = \nabla_{\tilde{\mathbf{x}}} \cdot R^T \mathbf{D}^{(k)} R \nabla_{\tilde{\mathbf{x}}}. \tag{4.5}$$

Since $\mathbf{D}^{(k)}$ is assumed positive definite, we can let $R = P(\tilde{\mathbf{D}}^{(k)})^{-1/2}$. Under this change of variable the differential operator becomes a standard Laplacian from Eq. (4.5),

$$\nabla_{\mathbf{x}} \cdot \mathbf{D}^{(k)} \nabla_{\mathbf{x}} = \Delta_{\tilde{\mathbf{x}}}. \tag{4.6}$$

Since the operators $\nabla_{\mathbf{x}} \cdot \mathbf{D}^{(k)} \nabla_{\mathbf{x}}$ are decoupled, we introduce for the concentration field of each chemical species a separate coordinate system $\tilde{\mathbf{x}}^{(k)} = R^{(k)}\mathbf{x}$ and let $c_k = c_k(\tilde{\mathbf{x}}^{(k)}, t)$. With the choice $R^{(k)} = P^{(k)}(\tilde{\mathbf{D}}^{(k)})^{-1/2}$ the full differential operator becomes a standard Laplacian

$$\nabla_{\mathbf{x}} \cdot \mathbf{D}\nabla_{\mathbf{x}} = \Delta_{\tilde{\mathbf{x}}}. \tag{4.7}$$

To simplify the discussion, we assume throughout that this coordinate transformation is made to Eq. (2.2) before numerical approximation.

5. Meshes with multiple levels of resolution

In many reaction–diffusion systems, interesting features are exhibited only in a sub-region of the spatial domain, such as in a chemically active front or in a layer near boundaries [33,51,52]. For such systems we introduce discretizations based on meshes which allow for multiple levels of resolution. Two important issues arise in the context of SPDEs which are not present in the deterministic PDE setting. The first issue is the need for consistent discretizations of the stochastic driving field at coarse-refined interfaces of the mesh, where there are changes in the spatial resolution of the mesh. The second issue is the need for efficient methods to generate efficiently the required stochastic driving fields on such meshes. We discuss discretizations for the Laplacian on multilevel meshes and then introduce stochastic numerical methods addressing these two issues.

5.1. Discretization of the Laplacian on multilevel meshes

To obtain discretizations on multilevel meshes, we express the Laplacian in terms of the gradient and divergence operators

$$\Delta = \mathcal{D}\mathcal{G} \quad : \text{Laplacian Operator} \tag{5.1}$$

$$\mathcal{D} = \nabla \cdot \quad : \text{Divergence Operator} \tag{5.2}$$

$$\mathcal{G} = \nabla \quad : \text{Gradient Operator} \tag{5.3}$$

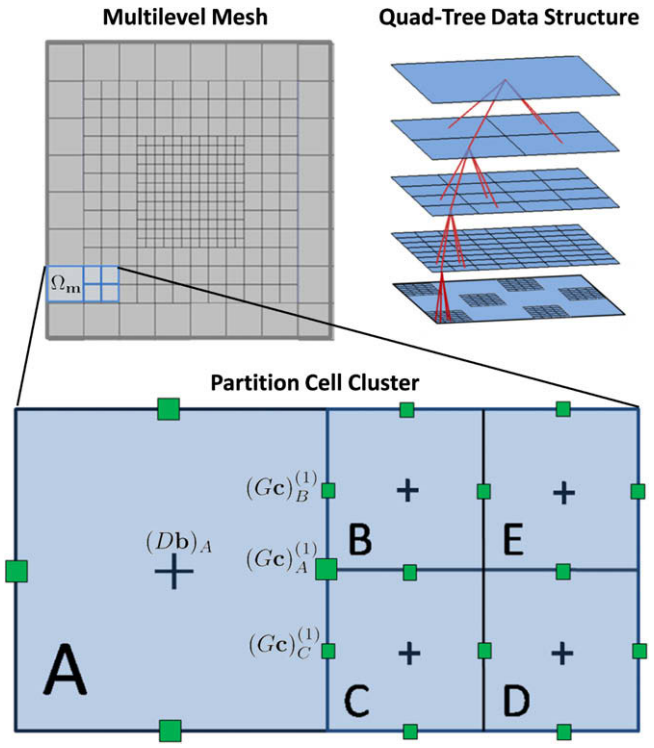

Fig. 5.1. Meshes with multiple levels of resolution. The mesh defines a discretization of space into a collection of square partition cells $\Omega_{\mathbf{m}}$ index by $\mathbf{m}$, (upper left). For discretizations approximating the divergence and gradient differential operators, values are stored at both the center of each partition cell and at the centers of the faces of each partition cell. The cell center data is denoted by + and the face centered data is denoted by □. Discretizations must handle the coarse-refined interfaces of the mesh where there is a change in spatial resolution. For this purpose, a partition cell cluster is defined which consists of the coarse partition cell *A* and its four neighbors in the direction of the interface *BCDE*, (lower panel). For the face of *A* shared with *BC*, we assume the face centered value of *A* is the average of the face centered values of *BC*. The partition with different levels of spatial resolution is represented using a data structure based on quad-trees (upper right).

To approximate the operators, we define for any discretization mesh a partition of the spacial domain $\{\Omega_{\mathbf{m}}\}_{\mathbf{m}}$, see Fig. 5.1. For a given partition cell $\Omega_{\mathbf{m}}$ we allow for numerical values to be defined both at the center of the partition cell and at the center of the faces of the partition cell. We approximate the Divergence Operator $\mathcal{D}$ at the center of a partition cell using

$$(D\mathbf{b})_{\mathbf{m}} = \frac{1}{\Delta x_{\mathbf{m}}} \sum_{k=1}^{4} \mathbf{b}_{\mathbf{m},k} \cdot \mathbf{n}_{\mathbf{m},k}. \tag{5.4}$$

The term $\mathbf{b}_{\mathbf{m},k}$ denotes the vector value at the center of the kth face of the partition cell $\Omega_{\mathbf{m}}$. The $\mathbf{b}$ denotes the composite vector of all such values on the partition. The $\mathbf{n}_{\mathbf{m},k}$ denotes the outward normal to the kth face of the partition cell. The term $\Delta x_{\mathbf{m}}$ is the width of the partition cell. The notation $(\cdot)_{\mathbf{m}}$ denotes the component corresponding to the value at the center of the partition cell with index $\mathbf{m}$. A useful property of this approximation to the divergence operator is that its evaluation only requires at the face centers the components in the normal direction, see the dot product in Eq. (5.4).

We approximate the Gradient Operator $\mathcal{G}$ at the center of the faces of each partition cell. Given the different levels of resolution in the mesh, many cases can arise in principle. By convention, we restrict our methods to deal with meshes which have the nested property that neighboring cells differ in resolution by at most one level. This requires only two cases be considered at each face of a partition cell. The first is when the neighboring cell is at the same level of spatial resolution. This corresponds to $\Delta x_{\mathbf{m}} = \Delta x_{\ell_k}$, where ℓ_k denotes the index of the neighbor in the direction of the kth face of the partition cell. The second is when the neighboring cells differ by one level of resolution, $\Delta x_{\mathbf{m}} = 2\Delta x_{\ell_k}$ or $\Delta x_{\mathbf{m}} = \frac{1}{2}\Delta x_{\ell_k}$.

To approximate the gradient operator on a face shared with a neighbor at the same level of resolution, we use

$$(G\mathbf{c})_{\mathbf{m},k}^{(k)} = \operatorname{sign}(\mathbf{n}_{\mathbf{m},k}^{(k)}) \frac{\mathbf{c}_{\ell_k} - \mathbf{c}_{\mathbf{m}}}{\Delta x_{\mathbf{m}}}. \tag{5.5}$$

In the notation $(\cdot)_{\mathbf{m},k}$ denotes the components corresponding to the vector value at the center of the kth face of the partition cell with index $\mathbf{m}$. The notation $(\cdot)^{(k)}$ denotes the kth vector component. The discrete gradient operator only defines the kth vector component at each face since this is all that is required by the discrete divergence operator D of Eq. (5.4).

To approximate the gradient operator on faces shared between neighbors differing by one level of spatial resolution, we must consider a cluster of partition cells. To simplify the discussion, we consider the case where the partition cell with index

$\mathbf{m}$ has neighbors at the kth face which are of a more refined level of resolution, $\Delta x_{\mathbf{m}} = 2\Delta x_{\ell_k}$. We define the cluster to be the collection of partition cells consisting of the partition cell with index $\mathbf{m}$ (labeled A) and the four neighboring partition cells in the direction of the outward normal of the kth face (labeled B, C, D, E), see Fig. 5.1. The components of the gradient operator are approximated by

$$(G\mathbf{c})_B^{(k)} = \text{sign}(\mathbf{n}_{\mathbf{m},k}^{(k)}) \frac{\frac{1}{2}(\mathbf{c}_B + \mathbf{c}_C) - \mathbf{c}_A}{\frac{3}{4}\Delta x_{\mathbf{m}}}, \tag{5.6}$$

$$(G\mathbf{c})_C^{(k)} = \text{sign}(\mathbf{n}_{\mathbf{m},k}^{(k)}) \frac{\frac{1}{2}(\mathbf{c}_B + \mathbf{c}_C) - \mathbf{c}_A}{\frac{3}{4}\Delta x_{\mathbf{m}}}, \tag{5.7}$$

$$(G\mathbf{c})_A^{(k)} = \frac{1}{2}\left[(G\mathbf{c})_B^{(k)} + (G\mathbf{c})_C^{(k)}\right]. \tag{5.8}$$

To obtain a discretization of the Laplacian Δ on meshes with multiple levels of resolution, we use the approximation

$$L = DG. \tag{5.9}$$

The discrete gradient operator G and discrete divergence operator D are defined by Eqs. (5.4)–(5.7) and (5.8). Similar discretizations have been used in [14–16].

Using this approach to discretize the Laplacian allows for both Neumann and Dirichlet boundary conditions to be imposed readily on rectangular domains. For Neumann conditions the domain is discretized so that faces of the partition cells align with the domain boundary. To impose the Neumann conditions the values of components of the gradient are specified at the center of faces of the partition coinciding with the boundary. For Dirichlet boundary conditions the domain is discretized so that the centers of the partition cells align with the domain boundary. To impose the Dirichlet boundary conditions the values are specified at the center of partition cells coinciding with the boundary. The Laplacian is then computed using Eq. (5.9), where the range of the gradient and divergence operators are restricted to the non-boundary values of the partition cells.

5.2. Discretization of the stochastic driving field on multilevel meshes

For the development of stochastic numerical methods approximating Eq. (2.2) the stochastic driving field $\mathbf{n}$ must be discretized both in space and in time. On multilevel meshes, obtaining useful discretizations for the stochastic driving field encounter a number of issues. One issue is to obtain spatial discretizations of the stochastic driving field which handle coarse-refined interfaces of the mesh, where there are changes in the spatial resolution of the mesh. Another issue is to develop methods which can generate efficiently the discretized stochastic fields on the multilevel mesh with the required covariance structure.

To handle coarse-refined interfaces, we derive spatial discretizations using the fluctuation–dissipation principle established for the discrete system in Eq. (2.4) of Section 2. We obtain a discretization by considering how equilibrium fluctuations of the discrete system approximate the equilibrium fluctuations of the continuum system. We require the discrete system have equilibrium fluctuations with covariance C given by

$$C_{\ell,\mathbf{m}} = \frac{\overline{C}}{\Delta x_{\mathbf{m}}^2}\delta_{\ell,\mathbf{m}}, \tag{5.10}$$

where $\overline{C}_{ij} = \bar{c}_i\delta_{ij}$ and $\bar{c}_i = \langle c_i \rangle$. This choice of covariance C corresponds to the equilibrium fluctuations of the continuum system obtained when solutions are spatially averaged over each of the partition cells, see Eq. (3.1).

To obtain a spatial discretization of the stochastic driving field, we use this C and the fluctuation–dissipation principle established by Eq. (3.10). This requires the covariance Γ of the stochastic driving field satisfy

$$\Gamma = -2LC. \tag{5.11}$$

To obtain this expression, we have used that the product LC is symmetric for the specific choice of covariance C given in Eq. (5.10) and discretization of the Laplacian L given in Eq. (5.9). This provides one approach for obtaining a spatial discretizations for the stochastic driving field on multilevel meshes handling the coarse-refined interfaces. We compare this spatial discretization with other choices in Section 6.

The stochastic driving field must also be discretized in time. The SPDE given in Eq. (2.2) is approximated by the following stochastic process, see Section 3,

$$d\mathbf{c}_t = L\mathbf{c}_t dt + \mathbf{f}dt + Qd\mathbf{B}_t, \tag{5.12}$$

$$QQ^T = \Gamma. \tag{5.13}$$

To obtain a numerical approximation of Eq. (2.2), the stochastic process of Eq. (5.12) must be discretized in time. We use the Euler–Maruyama Method [10] which gives the discretization

$$\mathbf{c}^{n+1} = \mathbf{c}^n + L\mathbf{c}^n\Delta t + \mathbf{f}^n\Delta t + \boldsymbol{\eta}^n. \tag{5.14}$$

The $\mathbf{c}^n$ denotes the composite vector of concentrations of the molecular species over the mesh at time $t_n = n\Delta t$. The time-step is denoted by Δt. The term $\boldsymbol{\eta}^n$ denotes a vector-valued Gaussian random variate with mean zero and covariance

$$\langle (\boldsymbol{\eta}^m)(\boldsymbol{\eta}^n)^T \rangle = \Gamma \Delta t \delta_{m,n}. \tag{5.15}$$

For the precise definition of the covariance Γ of $\boldsymbol{\eta}$, reference the Eqs. 5.11, 5.10 and 5.9. The random variates $\boldsymbol{\eta}$ provide the discretization both in space and in time for the stochastic driving field $\mathbf{n}$ of Eq. (2.2). For numerical methods based on this approach, an important issue is whether the variates $\boldsymbol{\eta}$ can be generated efficiently on the multilevel mesh with the required covariance given in Eq. (5.15). For other possible temporal discretizations, see [10,13].

5.3. Generation of the discretized stochastic driving fields on multilevel meshes

Efficient generation methods are needed for the random variates of the discretized stochastic driving field $\boldsymbol{\eta}$ on the multilevel mesh. The variates $\boldsymbol{\eta}$ are Gaussian with mean zero and have covariance given by Eq. (5.15). To simplify the discussion we focus on methods to generate random variates $\mathbf{g}$ with covariance Γ given in Eq. (5.11). The random variates $\boldsymbol{\eta}$ can be generated readily from $\mathbf{g}$, since the covariances of $\boldsymbol{\eta}$ and $\mathbf{g}$ differ only by a scalar factor. We also consider only the case of a single chemical species, since the stochastic driving field of each species is statistically independent. The methods naturally extend to the multiple chemical species case by generating the stochastic driving field for each species separately.

Our approach is based on splitting $\mathbf{g}$ into the sum of two other random variates $\mathbf{g}_1, \mathbf{g}_2$, with $\mathbf{g} = \mathbf{g}_1 + \mathbf{g}_2$. For such a splitting, the covariance $\mathbf{g}$ can be expressed as

$$\Gamma = \Gamma_{(1,1)} + \Gamma_{(2,2)} + \Gamma_{(1,2)} + \Gamma_{(2,1)}, \tag{5.16}$$

$$\Gamma_{(j,k)} = \langle \mathbf{g}_j \mathbf{g}_k^T \rangle. \tag{5.17}$$

The $\Gamma_{(j,k)}$ denotes the covariance of $\mathbf{g}_j$ with $\mathbf{g}_k$, for $j,k \in \{1,2\}$. If the two random variates $\mathbf{g}_1$ and $\mathbf{g}_2$ are independent then $\Gamma_{(1,2)} = \Gamma_{(2,1)} = 0$. This gives

$$\Gamma = \Gamma_1 + \Gamma_2. \tag{5.18}$$

For notational convenience, we denoted $\Gamma_1 = \Gamma_{(1,1)}$ and $\Gamma_2 = \Gamma_{(2,2)}$. This provides a useful link between matrix factorization of Γ and the splitting of a random variate $\mathbf{g}$ into the sum of two independent random variates. For such a matrix factorization to be of practical interest, the generation of $\mathbf{g}_1$ and $\mathbf{g}_2$ must be easier than the generation of $\mathbf{g}$. For the factorization to correspond to the splitting of a random variate $\mathbf{g}$, the factors Γ_1 and Γ_2 must be symmetric positive semidefinite in Eq. (5.18).

To obtain a factorization, we consider modification of the discrete divergence and gradient operators defined in Section 5.1. In the matrix representation of the discrete divergence operator, the matrix entries in each row correspond to weights for values at the face centers of the partition cells, see Eq. (5.4) and Fig. 5.1. We define the modified divergence operator D', by setting matrix entries to zero for weights corresponding to values at the center of faces shared along the coarse-refined interfaces. In the matrix representation of the discrete gradient operator G', the matrix entries correspond to weights for values at the centers of the partition cells, see Eqs. (5.5), (5.6), and Fig. 5.1. We define the modified gradient operator G', by setting matrix entries to zero for weights corresponding to values at the center of partition cells bordering immediately the coarse-refined interfaces.

With these modifications the discrete operators satisfy

$$G' = -D'^T. \tag{5.19}$$

A modified Laplacian can be defined by

$$L' = D'G' = -D'D'^T. \tag{5.20}$$

For the factorization of Γ, we use

$$\Gamma_1 = -2L'C, \tag{5.21}$$

$$\Gamma_2 = \Gamma - \Gamma_1. \tag{5.22}$$

For this to be useful, we must have that the factors Γ_1, Γ_2 are symmetric positive semidefinite and we must have efficient methods to generate $\mathbf{g}_1$ with covariance Γ_1 and $\mathbf{g}_2$ with covariance Γ_2.

To obtain methods to generate $\mathbf{g}_1$ with covariance Γ_1, we use properties of the modified discrete operators. An important property is that the matrices L', Γ_1, and C are all block diagonal for the same entries. This follows since the modified Laplacian corresponds to imposing Neumann boundary conditions at the coarse-refined interfaces. The Neumann boundary conditions serve to decouple domains with different levels of spatial resolution. As a result of decoupling, we obtain a collection of distinct domains each having a uniform level of spatial resolution. In Fig. 5.1 the mesh shown in the upper left has three such domains. We denote the block matrices by $L'^{(k)}, \Gamma_1^{(k)}$, and $C^{(k)}$, which each correspond to the domain with uniform spatial resolution indexed by k.

The block matrices of the covariance C have entries

$$C^{(k)}_{\ell,\mathbf{m}} = \frac{\bar{c}}{\Delta x^2_{\mathbf{m}}} \delta_{\ell,\mathbf{m}}, \quad \ell, \mathbf{m} \in \mathcal{J}_k. \tag{5.23}$$

The $\bar{c} = \langle c \rangle$ denotes the average concentration and in the case of a single species is a scalar, see Eq. (3.12). The $\mathcal{J}_k$ denotes the set of permitted indices for the entries of the kth block. Since the mesh resolution is uniform on the spatial domain corresponding to this block we have

$$C^{(k)} = \frac{\bar{c}}{\Delta x_k^2} I^{(k)}. \tag{5.24}$$

The $I^{(k)}$ is an identity matrix for the entries of the kth block, with zero entries elsewhere. We have used that on the kth spatial domain, $\Delta x_{\mathbf{m}} = \Delta x_k$ for all indices $\mathbf{m} \in \mathcal{J}_k$, where Δx_k is the uniform partition size. Results for the single species case extend naturally by generating independently the stochastic driving field for each chemical species.

The block matrices for Γ_1 can be expressed as

$$\Gamma_1^{(k)} = -2L'^{(k)}C'^{(k)} = (Q_1^{(k)})(Q_1^{(k)})^T, \tag{5.25}$$

$$Q_1^{(k)} = \left(\frac{\sqrt{2\bar{c}}}{\Delta x_k} D'^{(k)}\right). \tag{5.26}$$

This factorization allows for the variates $\mathbf{g}_1$ to be generated for each block by

$$\mathbf{g}_1^{(k)} = Q_1^{(k)} \boldsymbol{\xi}^{(k)}. \tag{5.27}$$

The $\boldsymbol{\xi}^{(k)}$ are standard Gaussian random variates with independent components having mean zero and variance one. The notation $[\cdot]^{(k)}$ denotes restriction to the vector components corresponding to the spatial domain with index k. In assignment of vector values using this notation, all of the non-indexed components are set to zero. We generate $\mathbf{g}_1$ by sweeping over all of the uniform spatial domains indexed by k to obtain

$$\mathbf{g}_1 = \sum_k \mathbf{g}_1^{(k)}. \tag{5.28}$$

This method provides an efficient means by which to generate the random variates $\mathbf{g}_1$.

To evaluate the cost of this procedure, we denote by N the number of components of partition cells. The procedure requires generating a total of N independent standard Gaussian random variates, performing a matrix-vector multiplication, and sweeping over the uniform spatial domains indexed by k. The generation of the Gaussian variates can be accomplished with $O(N)$ operations [63]. The matrix representation of the discrete divergence operator is sparse with a constant number of non-zero entries per row. Since $Q_1^{(k)}$ has the same sparse structure, the matrix-vector multiplications can be performed with a total of $O(N)$ operations. Using sparse data structures, the summation performed when sweeping over the uniform spatial domains can be performed with a total of $O(N)$ operations. This shows the method generates the random variate $\mathbf{g}_1^{(k)}$ with an optimal asymptotic cost of only $O(N)$ operations.

To obtain methods to generate $\mathbf{g}_2$ with covariance Γ_2, we consider the remaining entries of Γ. By the definition of the modified discrete operators L', it can be shown that Γ_2 is block diagonal. In this case, the blocks correspond to each partition cell face involved in a coarse-refined interface. Associated with each such face is a cluster of partition cells consisting of one coarse cell and two refined cells which are immediate neighbors in the direction of the interface, see Fig. 5.1. The blocks are given by

$$\Gamma_2^{(j)} = \frac{8\bar{c}}{3\Delta x_j^2} M, \tag{5.29}$$

$$M = \begin{bmatrix} 1 & -2 & -2 \\ -2 & 4 & 4 \\ -2 & 4 & 4 \end{bmatrix}. \tag{5.30}$$

The faces of the coarse cells shared along the coarse-refined interface are indexed by j, see Fig. 5.1. The Δx_j denotes the width of the coarse partition cell of the cluster. An important technical point concerns partition cells which are involved in more than one cluster, such as at a corner, see Fig. 5.1. In this case, we use the convention that the repeated entries of the overlapping blocks for such partition cells are added together. This can be shown to give correctly the full matrix.

For the factorization given by Eq. (5.18) to be valid, the factor Γ_2 is required to be positive semidefinite. This property can be investigated by considering the eigenvalues of the matrix M. These are given by

$$\lambda_1 = 0, \quad \lambda_2 = 0, \quad \lambda_3 = 9. \tag{5.31}$$

This shows that Γ_2 is indeed positive semidefinite and the factorization is valid.

To generate the random variates $\mathbf{g}_2$, we use the eigenvectors of M. The orthonormal eigenvectors are given by

$$\mathbf{v}_1^{(j)} = \frac{1}{\sqrt{5}}\begin{bmatrix} 2 \\ 1 \\ 0 \end{bmatrix}, \quad \mathbf{v}_2^{(j)} = \frac{1}{3\sqrt{5}}\begin{bmatrix} 2 \\ -4 \\ 5 \end{bmatrix}, \quad \mathbf{v}_3^{(j)} = \frac{1}{3}\begin{bmatrix} 1 \\ -2 \\ -2 \end{bmatrix}. \tag{5.32}$$

The random variate is obtained for the cluster indexed by j by

$$\mathbf{g}_2^{(j)} = \sqrt{\frac{8\bar{c}}{3\Delta x_j^2}}\Big(\xi_1^{(j)}\sqrt{\lambda_1}\mathbf{v}_1^{(j)} + \xi_2^{(j)}\sqrt{\lambda_2}\mathbf{v}_2^{(j)} + \xi_3^{(j)}\sqrt{\lambda_3}\mathbf{v}_3^{(j)}\Big). \tag{5.33}$$

The $\xi_\ell^{(j)}$ denote independent standard Gaussian random variates with mean zero and variance one. This expression can be simplified since $\lambda_1 = \lambda_2 = 0$. This gives

$$\mathbf{g}_2^{(j)} = \frac{2\sqrt{6\bar{c}}}{\Delta x_j}\xi_3^{(j)}\mathbf{v}_3^{(j)}. \tag{5.34}$$

We generate $\mathbf{g}_2$ by sweeping over all of the clusters indexed by j to obtain

$$\mathbf{g}_2 = \sum_j \mathbf{g}_2^{(j)}. \tag{5.35}$$

This method provides an efficient means by which to generate $\mathbf{g}_2$.

To evaluate the cost of this procedure, we denote by N the number of partition cells. The generation procedure requires generating one Gaussian random variates for each cluster, a scalar-vector multiplication, and a sweep over the clusters index by j. By counting the number of clusters and using sparse data structures the procedure can be carried out with at most $O(N)$ computational operations. In practice, the actual cost is expected to be smaller since clusters only occur for partition cells at coarse-refined interfaces, which will typically make up only a small subset of the mesh. This method for generating $\mathbf{g}_2$ has an optimal asymptotic computational cost of $O(N)$ operations.

To generate the variate $\mathbf{g}$ we add the results from the procedure generating $\mathbf{g}_1$ and $\mathbf{g}_2$. Since this addition costs only $O(N)$ operations, we have shown that this method generates $\mathbf{g}$ with an optimal asymptotic computational cost of $O(N)$ operations. This method is significantly more efficient than commonly used approaches for correlated variates, such as Cholesky factorization [63]. The Cholesky algorithm applied to Γ costs $O(N^3)$ operations and generally produces a non-sparse factor [63]. Another drawback is that this factorization needs to be performed each time the structure of the adaptive mesh changes. For the generation of each random variate, a matrix-vector multiplication must be performed. Since the matrix factor is generally not sparse, each generation of a random variate costs $O(N^2)$ operations. The method using Eq. (5.22) performs significantly better than this, having instead a computational cost of only $O(N)$ operations.

In summary, the presented procedure for computing the random variate $\mathbf{g}$ by splitting it into two random variates $\mathbf{g}_1$ and $\mathbf{g}_2$ provides a potentially versatile tool for generating random variates with a specified covariance structure. The method relies on being able to factor the covariance Γ into Γ_1 and Γ_2 with random variates $\mathbf{g}_1$ and $\mathbf{g}_2$ which are easier to compute than $\mathbf{g}$. In the case of adaptive multilevel meshes such a factorization is found for the covariance Γ required by Eq. (5.11). In this case, the procedure is shown to have an optimal asymptotic computational cost of $O(N)$ operations.

5.4. Neumann and Dirichlet boundary conditions

In the case of Neumann and Dirichlet boundary conditions, the discretized stochastic driving fields have an adjusted covariance structure Γ. The covariance is adjusted by modifying the Laplacian operator L and covariance C appearing in Eq. (5.11). In the matrix representation of L and C the entries correspond to weights at the center of the partition cells.

For Dirichlet boundary conditions the domain is discretized so that the centers of the partition cells align with the domain boundary. To account for the Dirichlet boundary conditions, the covariance matrix C is modified to obtain $\widehat{C}$ by setting all entries to zero which correspond to the partition cells comprising the boundary. The covariance of the stochastic driving field is given by

$$\hat{\Gamma} = -2L\widehat{C}. \tag{5.36}$$

The stochastic driving field with covariance $\hat{\Gamma}$ is generated using the methods of Section 5.3.

For Neumann conditions the domain is discretized so that faces of the partition cells align with the domain boundary. To handle the Neumann boundary conditions, the discrete divergence operator D is modified to obtain $\check{D}$ by setting all entries to zero which correspond to faces of the partition cells which comprise the boundary. A modified Laplacian can be defined by $\check{L} = \check{D}G$. The covariance of the stochastic driving field is given by

$$\check{\Gamma} = -2\check{L}C. \tag{5.37}$$

The stochastic driving field with covariance $\check{\Gamma}$ is generated using the methods of Section 5.3.

We remark that the only cases considered were deterministic Neumann and Dirichlet boundary conditions. However, there may be applications in which stochastic boundary conditions are of interest. In this case, entries corresponding to the random fluxes or concentrations could be prescribed on the boundaries. The terms would contribute in the model through the use of boundary values in the evaluation of the discrete Laplacian appearing in Eq. (3.2). Depending on the system modeled, for such stochastic boundary conditions the stochastic driving field may require additional modification to yield consistency with statistical mechanics.

6. Equilibrium fluctuations at coarse-refined interfaces

Studies of the statistical features of a system often use stochastic numerical methods to generate a dynamical trajectory over a long period of time. The statistics are then estimated from the dynamical trajectory by performing an averaging over time, subject to ergodicity assumptions [2,3]. Statistics estimated in this manner include probability expectations corresponding to thermodynamic equilibrium and correlation functions in space and time [3]. For long trajectories, discretization errors are expected to accumulate significantly. The rate and nature of this accumulation is expected to play an important role in the accuracy of estimated statistics.

We investigate the contributing role of errors introduced by the spatial discretization of the stochastic driving field. We focus particularly on errors at the coarse-refined interfaces of a multilevel mesh. To highlight features of our approach to spatial discretization, and to highlight issues which can arise at such interfaces, we compare our approach with an alternative based on the use of random fluxes. For the different methods, we investigate the role of the accumulation of spatial discretization errors on the quality of the covariance of the equilibrium fluctuations of the discretized system at coarse-refined interfaces.

Each spatial discretization of the stochastic driving field which we consider, corresponds to a specific choice for the covariance Γ. For a given choice of Γ, the equilibrium fluctuations of the spatially discretized system have covariance

$$C = -\frac{1}{2}L^{-1}\Gamma. \tag{6.1}$$

We have used Eqs. (3.2) and (5.11).

As an alternative to the discretized stochastic driving field which we introduced in Section 5.2, we consider an approach based on random fluxes at the coarse-refined interface. For uniform meshes the stochastic driving field can be generated by taking the discrete divergence of independent random fluxes at the center of faces of the partition cells [5,7]. A natural extension to multilevel meshes is to introduce at the coarse-refined interface random fluxes at the face centers of the refined partition cells BC of each cluster, see Fig. 5.1. For the coarse partition cell A of each cluster, the total flux across the shared face into A is the sum of the fluxes at BC. This is represented in the area weighted fluxes by setting the face centered flux of the coarse cell to be the average of the random fluxes at BC.

To investigate the approach based on random fluxes for the discretization of the stochastic driving field, we construct Γ and use Eq. (6.1). It is found that while the discretization errors in the driving field are localized at the coarse-refined inter-

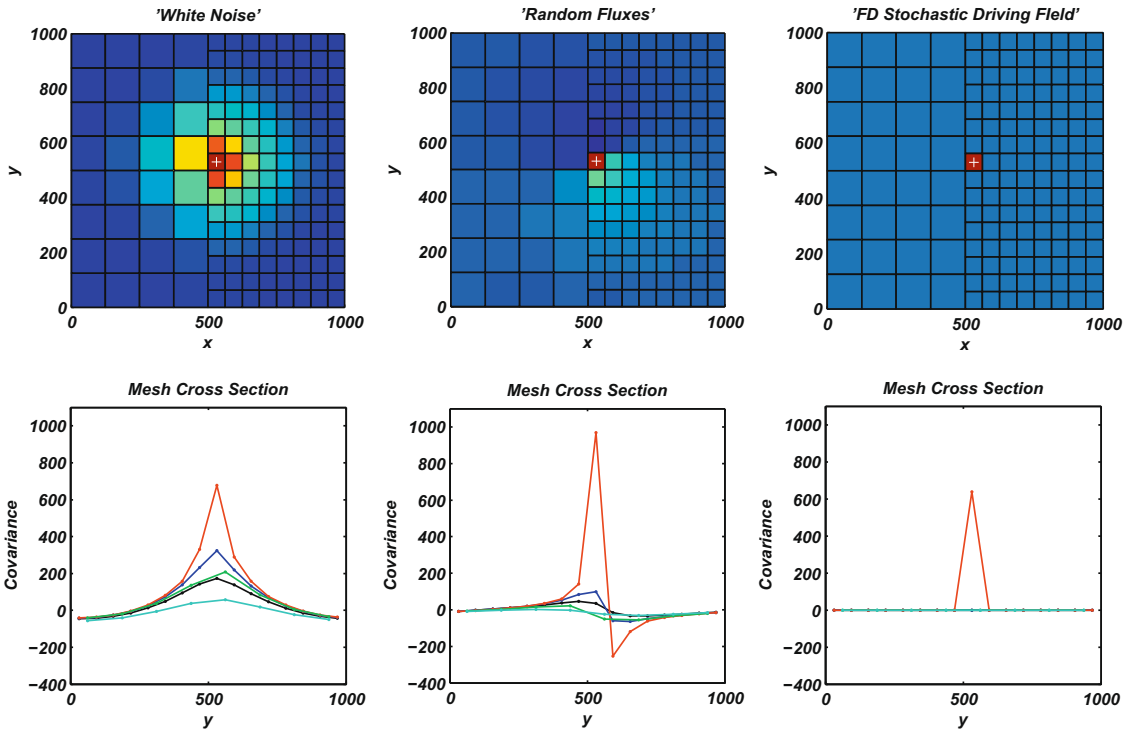

Fig. 6.1. Spatial covariance of equilibrium fluctuations at a coarse-refined interface. The top row shows the covariance of the equilibrium fluctuations of the system for each choice of the stochastic driving field at a cell at the coarse-refined interface on the refined side (see + symbol). In the second row, the covariance with this cell is plotted as a function of y at cross sections of the mesh near the interface.

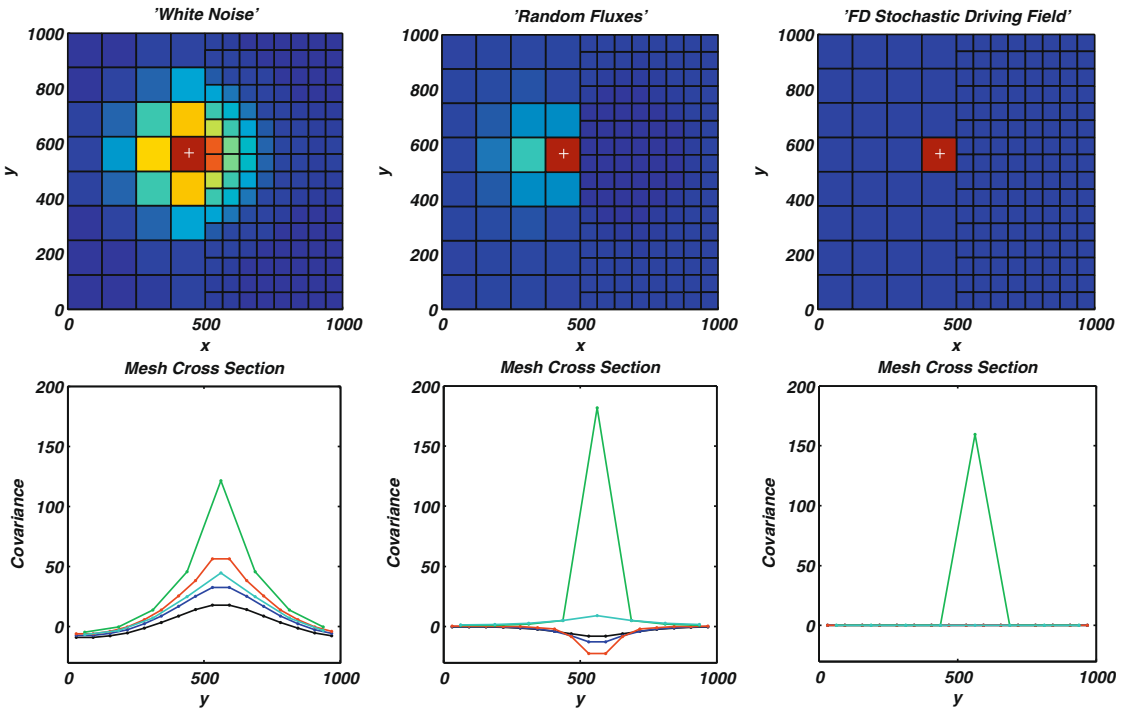

Fig. 6.2. The top row shows the covariance of the equilibrium fluctuations of the system for each choice of the stochastic driving field at a cell at the coarse-refined interface on the coarse side (see + symbol). In the second row, the covariance with this cell is plotted as a function of y at cross sections of the mesh near the interface. A color figure showing more clearly the fluctuations on the mesh is available in the on-line version of the paper.

face they contribute to the equilibrium fluctuations in a non-local manner. For the equilibrium fluctuations, this has the effect of introducing spatial correlations which extend several partition cells into the mesh away from the coarse-refined interface, see Figs. 6.1 and 6.2.

We investigate the propagation of localized errors at the coarse-refined interface. As a model for the spatial discretization error in the stochastic driving field we use a "white-noise" stochastic field. Since the equations are linear, the contributions of the errors in the stochastic driving field to the equilibrium fluctuations can be obtained from Eq. (6.1) with the special choice for Γ

$$\Gamma_{\ell,\mathbf{m}} = \delta_{\ell,\mathbf{m}}. \tag{6.2}$$

In this case, the resulting C gives the contributions of the errors to the equilibrium fluctuations. It is found that while the errors are localized and uncorrelated in space, they propagate over time and introduce long-range correlations in the covariance structure of the equilibrium fluctuations of the discrete system, see Figs. 6.1 and 6.2.

In contrast, our discretization of the stochastic driving field has by design equilibrium fluctuations with a prescribed covariance structure which is uncorrelated in space, see Eqs. (5.10), (5.11), and Figs. 6.1 and 6.2. The discretization errors in this approach are constrained by requiring that the discrete system exhibit exactly the spatially averaged equilibrium fluctuations of the continuum system. While there are discretization errors with respect to the continuum stochastic driving field, the constraints introduce errors which propagate on the mesh in such a manner that they do not introduce long-range correlations in the equilibrium fluctuations of the system. When compared with the discretization based on random fluxes, this feature is expected to give more accurate results for the estimation of spatial correlation functions of the system.

The approach we introduce for controlling the errors contributed by spatial discretization of the stochastic driving field is potentially useful in developing stochastic numerical methods for many types of SPDEs. The approach provides a method by which to spatially discretize the stochastic driving fields by controlling the errors in the fluctuations of the discretized system at statistical steady-state. We further highlight features of this approach to spatial discretization in the convergence analysis developed in Section 8.

7. Meshes with curved boundaries

For many applications it is natural to consider reaction–diffusion systems on spatial domains having a geometry with curved boundaries. In pattern forming systems the geometry along with boundary conditions are expected to play an important role. The geometry is expected to effect the possible eigenmodes of the system and constrain perturbations which effect

stability [49,51,52]. In biological applications, it is expected that the location within a cell or tissue may dramatically effect the rates of diffusivity and reactivity of the chemical species. One natural modeling approach is to decompose space into disjoint but coupled domains on which separate reaction–diffusion equations are parameterized and solved to account for local effects [52]. For biological systems, the individual regions are expected to have complicated geometries [1,73]. The discretizations introduced previously for the Laplacian on structured multilevel meshes only allow for rectangular boundaries, see Section 5. We extend the applicability of the presented methods by developing discretizations for domains with curved boundaries.

7.1. Discrete approximation of the Laplacian on meshes with curved boundaries

To obtain accurate results for the Laplacian on domains with non-rectangular geometries requires the development of appropriate discretizations in the vicinity of the curved boundaries. To simplify the discussion, we consider geometries which have only smooth boundaries. We also only consider the case of Neumann boundary conditions imposed on the curved boundary. Our approach is based on a finite volume discretization of the Laplacian and is a variant of the methods referred to as *Embedded Boundary Methods*, *Cartesian Grid Methods*, *Cut-Cell Methods*, see [17–23].

The boundary is approximated over the regular structured mesh by piecewise linear segments. The linear segments are defined by connecting the points of intersection of the boundary with the faces of the partition cells $\{\Omega_{\mathbf{m}}\}$, see Fig. 7.1. We refer to any partition cell containing a linear boundary segment as a "cut-cell." From the assumed smoothness of the boundary, it is always possible to refine sufficiently the mesh so that each partition cell contains at most one linear boundary segment. For each cut-cell of the boundary $\Omega_{\mathbf{m}}$, two sub-regions are defined. The first sub-region corresponds to the part inside the solution domain of the reaction–diffusion system and is denoted by $\Omega'_{\mathbf{m}}$. The second corresponds to the region outside the solution domain and is denoted by $\Omega''_{\mathbf{m}}$. The full partition cell is always assumed to be the union of these two parts, $\Omega_{\mathbf{m}} = \Omega'_{\mathbf{m}} \cup \Omega''_{\mathbf{m}}$.

To obtain a discretization of the Laplacian, we use the Gauss Divergence Theorem on each partition cell [66]

$$\int_{\Omega'_{\mathbf{m}}} \Delta c d\mathbf{x} = \int_{\partial\Omega'_{\mathbf{m}}} J dA_{\mathbf{x}}, \tag{7.1}$$

$$J = -\nabla c \cdot \mathbf{n}. \tag{7.2}$$

The $\mathbf{n}$ denotes the inward normal on the partition boundary $\partial\Omega'_{\mathbf{m}}$. The $\Omega'_{\mathbf{m}}$ refers to the part of the partition cell inside the solution domain. The J denotes the inward concentration flux across the face per unit length.

A discretization is obtained for the Laplacian by approximating the two sides of Eqs. (7.1) and (7.2). By treating the Laplacian as constant on each partition cell and the concentration gradient as constant on each partition face, we obtain the discretization

$$[Lc]_{\mathbf{m}} = \frac{1}{|\Omega'_{\mathbf{m}}|} \sum_k J^{[k]}_{\mathbf{m}} |\partial\Omega'_{\mathbf{m},k}|. \tag{7.3}$$

The $|\Omega'_{\mathbf{m}}|$ denotes the area of the inside sub-region of the partition cell indexed by $\mathbf{m}$. The $|\partial\Omega'_{\mathbf{m},k}|$ denotes the length of the kth face of the inside sub-region of the partition cell. The $J^{[k]}_{\mathbf{m}}$ denotes the concentration flux across the kth face into the interior sub-region.

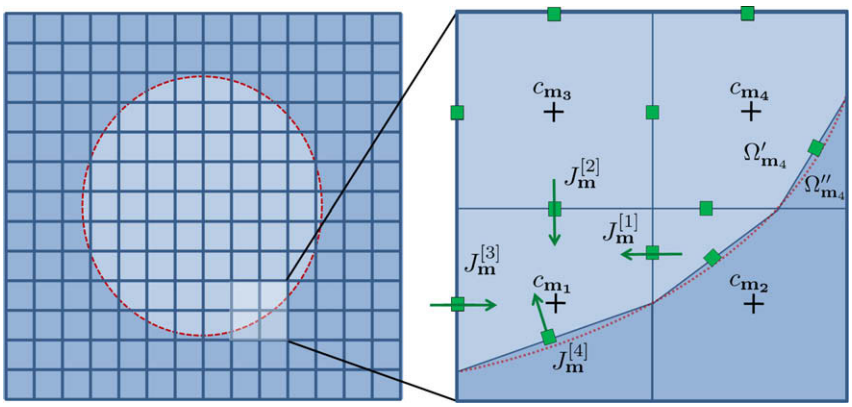

Fig. 7.1. Domain with a curved boundary and cut-partition cells: on the left is shown the disk-shaped domain for the reaction–diffusion system. On the right is shown for a cut cell, partition cells of the mesh used for computing the concentration flux $J^{[1]}_{\mathbf{m}}$. The symbol + denotes the location of the center of the full partition cells. The symbol □ denotes the location of the center of the faces of the partition cells. For cut faces, the center is located at the mid-point of the face segment inside the solution domain. The light region denotes for the partition cells the sub-regions $\Omega'_{\mathbf{m}}$ inside the solution domain. The dark region denotes for the partition cells the sub-regions $\Omega''_{\mathbf{m}}$ outside the solution domain. On the right are shown for the interior sub-region $\Omega'_{\mathbf{m}_1}$ the inward concentration fluxes labeled by $J^{[k]}_{\mathbf{m}}$.

The concentration field of the chemical species is represented by values at the center of each full partition cell, even when the partition cell is cut by a boundary. This center value is used even when the full partition cell center falls within the exterior sub-region $\Omega''_{\mathbf{m}}$. In this latter case, the value at the cell center can be thought of as representing the extrapolation of a smooth concentration field solution into the exterior sub-region. This approach of using values at the center of the full partition cell is based on the work of [23].

For the discretization in Eq. (7.3) to be useful, accurate estimates are required for the concentration fluxes $J^{[k]}_{\mathbf{m}}$. Estimates are needed only for the faces aligned with the Cartesian directions. The concentration flux on the curved boundary is specified since we are only considering the case of Neumann boundary conditions. To estimate the concentration flux at a given face, a bilinear interpolation is made to define locally a concentration field

$$\begin{aligned}
&\tilde{c}^{[k]}(\mathbf{x}) = \alpha\beta c_{\mathbf{m}_1} + (1-\alpha)\beta c_{\mathbf{m}_2} + \alpha(1-\beta)c_{\mathbf{m}_3} + (1-\alpha)(1-\beta)c_{\mathbf{m}_4},\\
&\alpha(\mathbf{x}) = (\mathbf{x}^{(1)}_2 - \mathbf{x}^{(1)})/\Delta x,\\
&\beta(\mathbf{x}) = (\mathbf{x}^{(2)}_4 - \mathbf{x}^{(2)})/\Delta x.
\end{aligned} \tag{7.4}$$

For the $\mathbf{m}$th partition cell and kth face we assign $\mathbf{m}_1 = \mathbf{m}$. The other indices $\mathbf{m}_2, \mathbf{m}_3, \mathbf{m}_4$ are assigned to the nearest neighbors in the direction of the kth face. For the collection of partition cells for the case of $k = 1$ and $k = 2$, see Fig. 7.1. The notation $(\cdot)^{(\ell)}$ refers to the vector component indexed by ℓ. The notation $(\cdot)^{[k]}$ refers to values associated with the face indexed by k. The flux is estimated by

$$J^{[k]}_{\mathbf{m}} = -\nabla\tilde{c}^{[k]}(\mathbf{x}_{k*}) \cdot \mathbf{n}^{[k]}_{\mathbf{m}}. \tag{7.5}$$

The $\mathbf{x}_{k*}$ denotes the location of the center of the face, where the center location depends on how the face is cut by the boundary, see Fig. 7.1. The $\mathbf{n}^{[k]}_{\mathbf{m}}$ denotes the inward normal of the kth face.

Even though only linear interpolation was used, in fact the estimate is second order accurate for the flux evaluated at the center of faces aligned with the cartesian directions. We discuss this for the case of estimating $J^{[1]}_{\mathbf{m}}$, where the center of the face has component $\mathbf{x}^{(1)}_{1*} = \frac{1}{2}(\mathbf{x}^{(1)}_2 + \mathbf{x}^{(1)}_1)$. In the case of a full partition cell where the face is not cut, Eq. (7.5) yields the usual central difference approximation for the gradient component in the x-direction

$$J^{[1]}_{\mathbf{m}} = \frac{c_{\mathbf{m}_2} - c_{\mathbf{m}_1}}{\Delta x}. \tag{7.6}$$

This shows the estimate is second order accurate in the case of an uncut cell.

In the case of a partition cell in which a face is cut, the estimate corresponds to a linear interpolation in the y-direction of two central difference approximations for the gradient component in the x-direction, see Eqs. (7.4) and (7.5),

$$J^{[1]}_{\mathbf{m}} = \beta\frac{c_{\mathbf{m}_2} - c_{\mathbf{m}_1}}{\Delta x} + (1-\beta)\frac{c_{\mathbf{m}_4} - c_{\mathbf{m}_3}}{\Delta x}. \tag{7.7}$$

Since each central difference is second order accurate, the linear interpolation ensures the estimate at the face center is also second order accurate. Using these estimates in Eq. (7.3) yields a first order accurate discretization of the Laplacian. For a more detailed discussion, see [23].

At curved boundaries we use the discretization for the Laplacian defined by Eqs. 7.3, 7.4 and 7.5. For the approximation of the SPDEs given in Eq. (2.2), the stochastic driving field must be discretized at the curved boundaries. Approximation at curved boundaries poses a challenge, since the partition cells have non-homogeneous areas and geometries defined by the boundary. This irregularity must be handled in the discretization of the stochastic driving field. For a discretization to be useful in practice, methods are needed for the efficient generation of random variates with the required covariance structure representing the discrete stochastic driving field.

7.2. Discretization of the stochastic driving field on meshes with curved boundaries

To discretize the stochastic driving field on meshes with curved boundaries, we take an approach similar to the case of multilevel meshes discussed in Section 5. The approach uses the fluctuation–dissipation principle established for the discrete system in Eq. (3.10). The curved boundary introduces irregular terms in the discretizations as a result of the non-homogeneous areas and face lengths of the cut partition cells. To obtain a consistent spatial discretization of the stochastic driving field, the covariance of the equilibrium fluctuations C is specified to be

$$C_{\ell,\mathbf{m}} = \frac{\overline{C}}{|\Omega'_{\mathbf{m}}|}\delta_{\ell,\mathbf{m}}. \tag{7.8}$$

The $\overline{C}_{ij} = \bar{c}_i\delta_{ij}$ and $\bar{c}_i = \langle c_i\rangle$ is the average concentration of the ith chemical species. For each partition cell, the $|\Omega'_{\mathbf{m}}|$ is the area of the sub-region within the solution domain. This choice of covariance C corresponds to the equilibrium fluctuations of the continuum system obtained when the concentration field is spatially averaged over the interior sub-region of each partition cell, see Eq. (3.1).

For the choice of equilibrium covariance C in Eq. (7.8) and the discrete Laplacian L in Eq. (7.3), the discretized stochastic driving field has the covariance Γ given by

$$\Gamma = -LC - CL^T. \tag{7.9}$$

The stochastic driving field must also be discretized in time. The SPDE given in Eq. (2.2) is approximated by the following stochastic process, see Section 3,

$$d\mathbf{c}_t = L\mathbf{c}_t dt + \mathbf{f} dt + Q d\mathbf{B}_t, \tag{7.10}$$

$$QQ^T = \Gamma. \tag{7.11}$$

To obtain a numerical approximation of Eq. (2.2), the stochastic process of Eq. (7.11) must be discretized in time. We use the Euler–Maruyama Method [10] which gives the discretization

$$\mathbf{c}^{n+1} = \mathbf{c}^n + L\mathbf{c}^n \Delta t + \mathbf{f}^n \Delta t + \boldsymbol{\eta}^n. \tag{7.12}$$

The $\mathbf{c}^n$ denotes the composite vector of concentrations of the molecular species over the mesh at time $t_n = n\Delta t$. The time-step is denoted by Δt. The term $\boldsymbol{\eta}^n$ denotes a vector-valued Gaussian random variate with mean zero and covariance

$$\langle (\boldsymbol{\eta}^m)(\boldsymbol{\eta}^n)^T \rangle = \Gamma \Delta t \delta_{m,n}. \tag{7.13}$$

For the precise definition of the covariance Γ of $\boldsymbol{\eta}$, reference the Eqs. 7.9, 7.8 and 7.3. The random variates $\boldsymbol{\eta}$ provide the discretization both in space and in time for the stochastic driving field $\mathbf{n}$ of Eq. (2.2). For numerical methods based on this approach, an important issue is whether the variates $\boldsymbol{\eta}$ can be generated efficiently on meshes with curved boundaries having the required covariance given in Eq. (7.13).

7.3. Generation of the discretized stochastic driving fields on meshes with curved boundaries

To obtain efficient generation methods for the variates of the discretized stochastic driving field $\boldsymbol{\eta}$ on meshes with curved boundaries, we use a splitting approach similar to the one used in Section 5.3. To simplify the discussion we focus on methods to generate random variates $\mathbf{g}$ with covariance Γ given in Eq. (7.9). The random variates $\boldsymbol{\eta}$ can be generated readily from $\mathbf{g}$, since the covariances of $\boldsymbol{\eta}$ and $\mathbf{g}$ differ only by a scalar factor.

To generate the random variate $\mathbf{g}$ we shall use the splitting $\mathbf{g} = \mathbf{g}_1 + \mathbf{g}_2$ into two independent random variates $\mathbf{g}_1, \mathbf{g}_2$. The covariance of $\mathbf{g}, \mathbf{g}_1$, and $\mathbf{g}_2$ then satisfy

$$\Gamma = \Gamma_1 + \Gamma_2. \tag{7.14}$$

For details of how this is obtained and notational conventions, see Section 5.3.

To obtain Γ_1 we consider a modified Laplacian. The discrete divergence operator has a matrix representation in which the entries correspond to weights on the faces of the partition cells. The modified divergence operator D'' is obtained by setting to zero all weights for faces shared with a cut partition cell. For the matrix representation, all rows are set to zero corresponding to cut partition cells. This defines a divergence operator D'' which is non-zero only on the domain consisting of the uncut partition cells. We similarly modify the discrete gradient operator to obtain G'' by setting to zero all weights associated with the cut-partition cells and faces shared with cut-partition cells.

An important property of the modified divergence and gradient is

$$D'' = -G''. \tag{7.15}$$

We define a modified Laplacian by

$$L'' = D''G'' = -D''(D'')^T. \tag{7.16}$$

The modified Laplacian is non-zero only on the domain of uncut partition cells. For this domain, the modification corresponds to imposing Neumann conditions on rectangular boundaries having a stair-case-like geometry. The factor Γ_1 is defined by

$$\Gamma_1 = -2L''C, \tag{7.17}$$

$$\Gamma_2 = \Gamma - \Gamma_1. \tag{7.18}$$

From Eq. (7.16) the factor Γ_1 can be explicitly factored using an approach similar to the one used in Section 5.3, see Eq. (5.26). The explicit factorization also allows for a similar generation method to be used for the random variates, see Section 5.3. The computational cost of generating the random variates by these methods is $O(N)$ operations, where N is the total number of partition cells.

To obtain Γ_2 we consider the remaining entries of the covariance. This factor is more difficult to handle since the entries are irregular. The entries correspond to weights over the cell centers of cut-partition cells which have different areas and geometries. The covariance matrix Γ_2 can be shown to be block diagonal. Each block is denoted by $\Gamma_2^{(q)}$ and corresponds to each disjoint collection of partition cells which are cut by the boundaries. The blocks $\Gamma_2^{(q)}$ can be shown to be positive semidefinite, which shows the splitting provides a valid factorization of Γ in Eq. (7.14). The semidefiniteness poses issues for the use of commonly used generation methods, such as the Cholesky factorization. The Cholesky factorization requires positive definiteness.

To handle this issue we use that $\Gamma_2^{(q)}$ is symmetric, which ensures a complete basis of orthonormal eigenvectors [61]. We generate the random variate using

$$\mathbf{g}_2^{(q)} = \sum_{k=1}^{M_q} \xi_k^{(q)} \sqrt{\lambda_k^{(q)}} \mathbf{v}_k^{(q)}. \tag{7.19}$$

The $\lambda_k^{(q)}$ denotes the kth eigenvalue and $\mathbf{v}_k^{(q)}$ denotes the kth orthonormal eigenvector. The $\xi_k^{(q)}$ denote independent Gaussian random variables with mean zero and variance one. The notation $(\cdot)^{(q)}$ refers to the vector components associated with the indices of the matrix block indexed by q. We denote by M_q the number of components of $\mathbf{g}_2^{(q)}$. To obtain the random variate $\mathbf{g}_2$, a sweep is made over all blocks

$$\mathbf{g}_2 = \sum_{q=1}^{n} \mathbf{g}_2^{(q)}. \tag{7.20}$$

We denote by n the total number of blocks.

To evaluate the cost of generating random variates, we consider each step of the above procedure. The eigenvalue and eigenvectors can be obtained for $\Gamma_2^{(q)}$ with a computational cost of $O(M_q^3)$ operations [61,67]. Since this must be performed for each block, the total cost of computing the eigenvectors and eigenvalues is $O(\sum_{q=1}^n M_q^3)$. While this has an unfavorable M_q^3 scaling, the number of partition cells M_q which are cut by the curved boundary comprise a lower one dimensional set and will often be only a small fraction of the partition cells of the mesh. Also, this eigenvector-eigenvalue procedure is only required when the geometry of the curved boundaries of the mesh change. For many problems this procedure is only required once at the beginning of a simulation.

To evaluate the cost of generating the random variate $\mathbf{g}_2^{(q)}$, the sum in Eq. (7.19) must be considered. In general, the eigenvectors will have almost all non-zero vector components. As a consequence the generation of each random variate $\mathbf{g}_2^{(q)}$ from the sum in Eq. (7.19) has a cost of $O(M_q^2)$ operations. Using sparse data structures, the sum in Eq. (7.20) can be evaluated with a cost of $O(\sum_{q=1}^n M_q)$ operations. Once the eigenvalues and eigenvectors are known, this gives for the generation of each random variate $\mathbf{g}_2$, the cost of $O(\sum_{q=1}^n M_q^2)$ operations.

The introduced methods allow for the generation of each random variate $\mathbf{g}$ with a computational cost of $O(N + \sum_{q=1}^n M_q^2)$, where N is the total number of partition cells in the mesh. Obtaining the required factors for the generation method has a computational cost of $O(N + \sum_{q=1}^n M_q^3)$. While the curved boundaries introduce a non-optimal M_q^2 and M_q^3 scaling in the methods, the introduced approach is still expected to be much more efficient than commonly used approaches. For instance, a direct eigenvector decomposition of Γ would cost $O(N^3)$ to generate the required factors and $O(N^2)$ to generate each random variate $\mathbf{g}$. The approach we introduce is significantly more efficient since the number of partition cells M_q which are cut by the curved boundary comprise a lower one dimensional set and will often be only a small fraction of N. This substantially reduces the size of the matrices for which the expensive eigenvector decomposition procedure must be performed and yields a more efficient generation procedure for $\mathbf{g}$.

8. Convergence of the stochastic numerical methods for the linearized equations

The proposed stochastic numerical methods are shown formally to converge in the case when the system is near steady-state and the fluctuations are small relative to the mean concentration. As discussed in Section 1, the solutions of Eq. (2.2) do not have classical solutions in terms of functions with well-defined pointwise values. Instead, the solutions are represented by linear functionals (distributions) [45,46,48]. To simplify the discussion and to avoid delving into too many technical issues, we formally demonstrate a form of weak convergence of the stochastic numerical methods which are semi-discretized in space. We consider bounds only in terms of the infinity norm, but it is expected that similar bounds can also be developed for the L^2-norm.

The form of weak convergence we consider corresponds to convergence of the moments of linear functionals A of the form

$$a(\mathbf{x}, t) = A[c] = \int_\Omega \int_0^t \alpha(\mathbf{x}, \mathbf{y}, s) c(\mathbf{y}, s) ds d\mathbf{y} \tag{8.1}$$

when numerically approximated by $\widetilde{A}$ of the form

$$\tilde{a}(\mathbf{x}, t) = \widetilde{A}[\mathbf{c}] = \sum_{\mathbf{m}} \int_0^t \alpha(\mathbf{x}, \mathbf{y}_{\mathbf{m}}, s) \tilde{c}_{\mathbf{m}}(s) ds \Delta x_{\mathbf{m}}^d. \tag{8.2}$$

The $\alpha(\mathbf{x}, \mathbf{y}, s)$ is a bounded compactly supported function which is smoothly varying in space $\mathbf{x}, \mathbf{y}$ and in time s. The form of weak convergence we consider is defined as convergence of all moments

$$\left\| \mathbf{M}^{(n)}_{\widetilde{A}_1, \widetilde{A}_2, \ldots, \widetilde{A}_n} - \mathbf{M}^{(n)}_{A_1, A_2, \ldots, A_n} \right\| \to 0, \quad \text{as } \Delta x \to 0. \tag{8.3}$$

The nth moment is defined by

$$\mathbf{M}^{(n)}_{A_1,A_2,\ldots,A_n}(\mathbf{x}_1,t_1,\mathbf{x}_2,t_2,\ldots,\mathbf{x}_n,t_n) = \langle a_1(\mathbf{x}_1,t_1)a_2(\mathbf{x}_2,t_2)\cdots a_n(\mathbf{x}_n,t_n)\rangle, \tag{8.4}$$

$$\mathbf{M}^{(n)}_{\widetilde{A}_1,\widetilde{A}_2,\ldots,\widetilde{A}_n}(\mathbf{x}_1,t_1,\mathbf{x}_2,t_2,\ldots,\mathbf{x}_n,t_n) = \langle \tilde{a}_1(\mathbf{x}_1,t_1)\tilde{a}_2(\mathbf{x}_2,t_2)\cdots \tilde{a}_n(\mathbf{x}_n,t_n)\rangle. \tag{8.5}$$

This convergence is required for each moment $n \geqslant 1$ and for any choice of functionals $A_1, A_2, \ldots, A_n$ of the form of Eq. (8.1) when approximated by $\widetilde{A}_1, \widetilde{A}_2, \ldots, \widetilde{A}_n$ of Eq. (8.2). The formal analysis will use the infinity-norm defined by

$$\|f(\mathbf{x}_1,t_1,\mathbf{x}_2,t_2,\ldots,\mathbf{x}_n,t_n)\|_\infty = \sup_{\mathbf{x}_1,\ldots,\mathbf{x}_n,t_1,\ldots,t_n} |f|. \tag{8.6}$$

The supremum is taken over the domain $\{\mathbf{x}_k \in \Omega, t_k \in [0,T]\}$, where both the spatial and temporal domains are bounded, $|\Omega| < \infty$ and $T < \infty$. The definition for convergence given by Eq. (8.3) is only one of many different types of convergence which can be defined for stochastic processes, see [10].

An intuitive motivation for this form of weak convergence is to think of the functionals A as being analogues of physical observations which would be obtained from experimental measurements of an underlying fluctuating concentration field. In experiments any measured quantity is averaged to some extent in space and time. Such averaging is represented in the functional by integrating the concentration field against the function α. Weak convergence corresponds to the situation where the statistics of any measurement of the underlying concentration field can be reproduced by simulations up to a specified precision provided one uses a sufficiently refined discretization mesh.

A number of simplifications can be made by utilizing linearity of the functional A and properties of c. From linearity and the smoothness of α we have that $a(\mathbf{x},t)$ is a Gaussian random field with well-defined pointwise values. This has the important consequence that statistics of the random field are completely determined by the first two moments. As a result, only the case of $n \leqslant 2$ needs to be considered in Eq. (8.3).

For the system close to statistical steady-state and for sufficiently small fluctuations relative to the mean concentration it is sufficient to consider the linearization of Eq. (2.2). This corresponds in Eq. (2.2) to a functional of the form $\mathbf{F}[c] = \mathcal{F}c$ where $\mathcal{F}$ denotes a linear functional. To simplify discussion of the formal analysis, for both the Laplacian and the linearized part of $\mathbf{F}$ we account for contributions in one linear operator $\mathcal{L}$ of the reaction–diffusion system. We denote the discretization of $\mathcal{L}$ by L.

In the linearized regime, taking an average of Eqs. (2.2) and (3.2) gives for the first moment a deterministic reaction–diffusion equation. For the first moments the convergence follows straight-forwardly from the deterministic convergence theory. We focus on demonstrating convergence of the second moments which arise from the fluctuations.

When working with the second moments it is helpful to consider the covariance function $\mathbf{R}(\mathbf{x}_1,t_1,\mathbf{x}_2,t_2) = \mathbf{M}^{(2)}_{A_1,A_2} - \mathbf{M}^{(1)}_{A_1}\mathbf{M}^{(2)}_{A_2}$, which can be expressed as

$$\begin{aligned}
&\mathbf{R}(\mathbf{x}_1,t_1,\mathbf{x}_2,t_2) = \int d\mathbf{y}_1 d\mathbf{y}_2 \int ds_1 ds_2 \alpha_1(\mathbf{x}_1,\mathbf{y}_1,s_1) q(\mathbf{y}_1,s_1,\mathbf{y}_2,s_2)\alpha_2(\mathbf{x}_2,\mathbf{y}_2,s_2),\\
&q(\mathbf{y}_1,s_1,\mathbf{y}_2,s_2) = \langle (c(\mathbf{y}_1,s_1)-\bar{c})(c(\mathbf{y}_2,s_2)-\bar{c})\rangle.
\end{aligned} \tag{8.7}$$

The α_1 and α_2 correspond to the linear functionals A_1 and A_2 represented in the form of Eq. (8.1). The integrals in $\mathbf{y}_1$, $\mathbf{y}_2$ and s_1, s_2 are taken over the bounded domain $\{(\mathbf{y}_1,\mathbf{y}_2,s_1,s_2) \in \Omega\times\Omega\times[0,t_1]\times[0,t_2]\}$. Similarly for the semi-discretized system we have the covariance function $\widetilde{\mathbf{R}}(\mathbf{x}_1,t_1,\mathbf{x}_2,t_2) = \mathbf{M}^{(2)}_{\widetilde{A}_1,\widetilde{A}_2} - \mathbf{M}^{(1)}_{\widetilde{A}_1}\mathbf{M}^{(2)}_{\widetilde{A}_2}$, which can be expressed as

$$\begin{aligned}
&\widetilde{\mathbf{R}}(\mathbf{x}_1,t_1,\mathbf{x}_2,t_2) = \sum_{\mathbf{m}_1}\sum_{\mathbf{m}_2}\int ds_1 ds_2 \alpha_1(\mathbf{x}_1,\mathbf{y}_{\mathbf{m}_1},s_1)\cdot\tilde{q}(\mathbf{y}_{\mathbf{m}_1},s_1,\mathbf{y}_{\mathbf{m}_2},s_2)\alpha_2(\mathbf{x}_2,\mathbf{y}_{\mathbf{m}_2},s_2)\Delta x^d_{\mathbf{m}_1}\Delta x^d_{\mathbf{m}_2},\\
&\tilde{q}(\mathbf{y}_{\mathbf{m}_1},s_1,\mathbf{y}_{\mathbf{m}_2},s_2) = \big\langle (\mathbf{c}_{\mathbf{m}_1}(s_1)-\bar{c})(\mathbf{c}_{\mathbf{m}_2}(s_2)-\bar{c})\big\rangle.
\end{aligned} \tag{8.8}$$

Since c is a solution of Eq. (2.2), we have formally that $c(\mathbf{y},s) = e^{(s-r)\mathcal{L}}c(\mathbf{y},r)$ when $s > r$. The $\mathcal{L}$ denotes the linearized operator which accounts for contributions from the Laplacian and linearized chemical reaction functional $\mathbf{F}$. The operator $\mathcal{L}$ is assumed to be negative semidefinite. The $e^{t\mathcal{L}}$ denotes the solution operator over the time interval $[0,t]$ from the semi-group associated with Eq. (2.2), see [46,54]. By the choice of stochastic driving field $\mathbf{n}$ in Eq. (2.1), we have

$$\langle (c(\mathbf{y}_1,s_1)-\bar{c})(c(\mathbf{y}_2,s_2)-\bar{c})\rangle = e^{(s_1-s_2)\mathcal{L}}\mathbf{C}, \tag{8.9}$$

for $s_1 \geqslant s_2$. We define $\mathbf{C}$ by

$$\mathbf{C}(\mathbf{y}_1,\mathbf{y}_2) = \bar{c}\delta(\mathbf{y}_1-\mathbf{y}_2). \tag{8.10}$$

Substituting this into Eq. (8.7) yields

$$\begin{aligned}
\mathbf{R}(\mathbf{x}_1,t_1,\mathbf{x}_2,t_2) = &\int d\mathbf{y}_1 d\mathbf{y}_2 \int_{s_1>s_2} ds_1 ds_2 \alpha_1(\mathbf{x}_1,\mathbf{y}_1,s_1)e^{(s_1-s_2)\mathcal{L}}\mathbf{C}\alpha_2(\mathbf{x}_2,\mathbf{y}_2,s_2)\\
&+\int d\mathbf{y}_1 d\mathbf{y}_2 \int_{s_2>s_1} ds_1 ds_2 \alpha_2(\mathbf{x}_2,\mathbf{y}_2,s_2)e^{(s_2-s_1)\mathcal{L}}\mathbf{C}\alpha_1(\mathbf{x}_1,\mathbf{y}_1,s_1).
\end{aligned}$$

By a similar argument for the semi-discretized Eq. (3.2) we have $\mathbf{c}(s) = e^{(s-r)L}\mathbf{c}(r)$ for $s > r$, where L denotes the discretized approximation for $\mathcal{L}$. The L is assumed to represent a negative semidefinite matrix. The e^{tL} denotes the matrix exponential

providing a solution operator for the spatially discretized equations, see [61,62]. By the choice of stochastic driving field $\mathbf{g}_t$ in Eq. (3.10), we have

$$\left\langle (\mathbf{c}(s_1)-\bar{\mathbf{c}})(\mathbf{c}(s_2)-\bar{\mathbf{c}})^T \right\rangle = e^{(s_1-s_2)L}C, \tag{8.11}$$

for $s_1 \geqslant s_2$. We define C by

$$[C]_{\mathbf{m}_1,\mathbf{m}_2} = \bar{c}\delta_{\mathbf{m}_1,\mathbf{m}_2}/\Delta x^d_{\mathbf{m}_1}. \tag{8.12}$$

The $\delta_{\mathbf{m}_1,\mathbf{m}_2}$ denotes a Kronecker δ-function. In the notation $[\cdot]_{\mathbf{m}_1,\mathbf{m}_2}$ denotes the $(\mathbf{m}_1,\mathbf{m}_2)$ matrix entry. Substituting this into Eq. (8.8) yields

$$\begin{aligned}\widetilde{\mathbf{R}}(\mathbf{x}_1,t_1,\mathbf{x}_2,t_2) = &\sum_{\mathbf{m}_1,\mathbf{m}_2}\int_{s_1>s_2} ds_1 ds_2 \alpha_1(\mathbf{x}_1,\mathbf{y}_{\mathbf{m}_1},s_1)\cdot[e^{(s_2-s_1)L}C]_{\mathbf{m}_1,\mathbf{m}_2}\alpha_2(\mathbf{x}_2,\mathbf{y}_{\mathbf{m}_2},s_2)\Delta x^d_{\mathbf{m}_1}\Delta x^d_{\mathbf{m}_2}\\ &+\sum_{\mathbf{m}_1,\mathbf{m}_2}\int_{s_2>s_1} ds_1 ds_2 \alpha_2(\mathbf{x}_2,\mathbf{y}_{\mathbf{m}_2},s_2)\cdot[e^{(s_2-s_1)L}C]_{\mathbf{m}_1,\mathbf{m}_2}\alpha_1(\mathbf{x}_1,\mathbf{y}_{\mathbf{m}_1},s_1)\Delta x^d_{\mathbf{m}_1}\Delta x^d_{\mathbf{m}_2}.\end{aligned}$$

To show convergence it is useful to let

$$\beta_1(\mathbf{y},t) = \int e^{(t-s_2)\mathcal{L}}\mathbf{C}(\mathbf{y},\mathbf{y}_2)\alpha_2(\mathbf{x}_2,\mathbf{y}_2,s_2)d\mathbf{y}_2, \tag{8.13}$$

$$\tilde{\beta}_1(\mathbf{y}_{\mathbf{m}},t) = \sum_{\mathbf{m}_2}[e^{(t-s_2)L}C]_{\mathbf{m},\mathbf{m}_2}\alpha_2(\mathbf{x}_2,\mathbf{y}_{\mathbf{m}_2},s_2)\Delta x^d_{\mathbf{m}_2} \tag{8.14}$$

with similar definitions for $\beta_2,\tilde{\beta}_2$. From the definitions of the operators $e^{(t-s_2)\mathcal{L}}$ and $e^{(t-s_2)L}$ we have that β_1 and $\tilde{\beta}_1$ solve the following differential equations with specified initial values

$$\left\{\begin{array}{ll}\partial\beta_1/\partial t = \mathcal{L}\beta_1, & \text{for } t > s_2\\ \beta_1(\mathbf{y},s_2) = \int \mathbf{C}(\mathbf{y},\mathbf{y}_2)\alpha_2(\mathbf{x}_2,\mathbf{y}_2,s_2)d\mathbf{y}_2 & \text{for } t = s_2\end{array}\right\} \tag{8.15}$$

and

$$\left\{\begin{array}{ll}d\tilde{\beta}_1/dt = L\tilde{\beta}_1, & \text{for } t > s_2\\ \tilde{\beta}_1(\mathbf{y}_{\mathbf{m}},s_2) = \sum_{\mathbf{m}_2}[C]_{\mathbf{m},\mathbf{m}_2}\alpha_2(\mathbf{x}_2,\mathbf{y}_{\mathbf{m}_2},s_2)\Delta x^d_{\mathbf{m}_2}, & \text{for } t = s_2\end{array}\right\}. \tag{8.16}$$

The β_2 and $\tilde{\beta}_2$ solve similar differential equations. Using the specific form of $\mathbf{C}$ and C given in Eqs. (8.10) and (8.12) we have that $\beta_1(\mathbf{y},s_2) = \alpha_2(\mathbf{x}_2,\mathbf{y},s_2)$ and $\tilde{\beta}_1(\mathbf{y}_{\mathbf{m}},s_2) = \alpha_2(\mathbf{x}_2,\mathbf{y}_{\mathbf{m}},s_2)$. From a deterministic convergence theory for the approximation of $\mathcal{L}$ by the discretized operator L for such differential equations, we have

$$\|\tilde{\beta}_1-\beta_1\| \to 0, \quad \text{as } \Delta x \to 0. \tag{8.17}$$

For β_2 and $\tilde{\beta}_2$ a similar result is obtained from the deterministic convergence theory.

The difference of the covariance functions of the discretized system and continuum system can be bounded using the triangle inequality by

$$\|\widetilde{\mathbf{R}}-\mathbf{R}\| \leqslant I_1+I_2+I_3+I_4, \tag{8.18}$$

where

$$\begin{aligned}I_1 &= \left\|\sum_{\mathbf{m}}\int_{s_1>s_2} ds_1 ds_2 \alpha_1(\mathbf{x}_1,\mathbf{y}_{\mathbf{m}},s_1)\Big(\tilde{\beta}_1(\mathbf{x}_1,\mathbf{y}_{\mathbf{m}},s_1)-\beta_1(\mathbf{x}_1,\mathbf{y}_{\mathbf{m}},s_1)\Big)\Delta x^d_{\mathbf{m}}\right\|\\ I_2 &= \left\|\sum_{\mathbf{m}}\int_{s_2>s_1} ds_1 ds_2 \alpha_2(\mathbf{x}_2,\mathbf{y}_{\mathbf{m}},s_2)\Big(\tilde{\beta}_2(\mathbf{x}_2,\mathbf{y}_{\mathbf{m}},s_2)-\beta_2(\mathbf{x}_2,\mathbf{y}_{\mathbf{m}},s_2)\Big)\Delta x^d_{\mathbf{m}}\right\|\\ I_3 &= \left\|\sum_{\mathbf{m}}\int_{s_2>s_1} ds_1 ds_2 \alpha_2(\mathbf{x}_2,\mathbf{y}_{\mathbf{m}},s_2)\beta_1(\mathbf{x}_1,\mathbf{y}_{\mathbf{m}},s_1)\Delta x^d_{\mathbf{m}} - \int d\mathbf{y}\int_{s_2>s_1} ds_1 ds_2 \alpha_2(\mathbf{x}_2,\mathbf{y},s_2)\beta_1(\mathbf{x}_1,\mathbf{y},s_1)\right\|\\ I_4 &= \left\|\sum_{\mathbf{m}}\int_{s_1>s_2} ds_1 ds_2 \alpha_1(\mathbf{x}_1,\mathbf{y}_{\mathbf{m}},s_1)\beta_2(\mathbf{x}_2,\mathbf{y}_{\mathbf{m}},s_2)\Delta x^d_{\mathbf{m}} - \int d\mathbf{y}\int_{s_1>s_2} ds_1 ds_2 \alpha_1(\mathbf{x}_1,\mathbf{y},s_1)\beta_2(\mathbf{x}_2,\mathbf{y},s_2)\right\|.\end{aligned} \tag{8.19}$$

Using properties of the norm, the I_1 term can be bounded by

$$I_1 \leqslant \left\|\sum_{\mathbf{m}}\int_{s_1>s_2} ds_1 ds_2 |\alpha_1(\mathbf{x}_1,\mathbf{y}_{\mathbf{m}},s_1)|\Delta x^d_{\mathbf{m}}\right\|\|\tilde{\beta}_1-\beta_1\|.$$

An important property of this estimate for I_1 is that the first term remains bounded as $\Delta x \to 0$. This follows since α_1 is compactly supported. Using this fact, we have $I_1 \to 0$ from Eq. (8.17). By a similar argument, we have $I_2 \to 0$.

For I_3 we have the first term is the Riemann sum approximation of the second integral term in $\mathbf{y}$, see Eq. (8.19). Since α_1 is compactly supported this implies $I_3 \to 0$. By a similar argument we have $I_4 \to 0$.

These arguments establish that $I_1, I_2, I_3, I_4 \to 0$ and formally show that

$$\|\widetilde{\mathbf{R}} - \mathbf{R}\| \to 0. \tag{8.20}$$

This along with convergence of the first moments implies

$$\|\mathbf{M}^{(2)}_{\widetilde{A}_1,\widetilde{A}_2} - \mathbf{M}^{(2)}_{A_1,A_2}\| \to 0. \tag{8.21}$$

Since the random fields are Gaussian and completely determined by the first two moments this analysis formally establishes that the stochastic numerical methods weakly converge. An important feature of this form of weak convergence is that the stochastic methods produce statistics convergent not only for individual observables represented by A. The stochastic methods are also convergent for any cross-correlation statistics for observables represented by A_1 and A_2 which reference the same underlying concentration field. Using the same basic approach, similar results are expected to hold for other norms, such as the L^2-norm.

To obtain convergent stochastic numerical methods, the analysis indicates that it is not only required that the discretization of the differential operator $\mathcal{L}$ be consistent, but that the discretized system have equilibrium fluctuations with a covariance structure C consistent with $\mathbf{C}$ of the continuum system. An important issue in practice is that the equilibrium covariance structure is not discretized independently but rather arises from the fluctuations induced by the discretized stochastic driving field, as in Eq. (3.2). To control the discretization errors introduced in the fluctuations of the discretized system as the mesh is refined, we utilized a variant of the fluctuation–dissipation principle of statistical mechanics, see Section 3. This was used to ensure that the stochastic numerical methods exhibit equilibrium fluctuations with the specified covariance C, which was chosen to be consistent with $\mathbf{C}$ of the continuum system. This approach is especially important at coarse-refined interfaces of multilevel meshes and cut-partition cells of the mesh near the domain boundaries to ensure discretizations for the stochastic driving field yield accurate stochastic numerical methods.

9. Applications

As a demonstration of the developed stochastic numerical methods, simulation studies are carried out for two applications. The first application studies the effect of fluctuations in microorganism direction sensing based on concentration gradients. The case investigated concerns a single biological cell which senses concentration gradients in an environment exhibiting a shallow gradient obscured by fluctuations. The second application studies fluctuation-induced pattern formation in spatially extended systems. A variant of the Gray–Scott chemical reactions is considered in a regime where the deterministic reaction–diffusion system only exhibits a localized stationary pattern. When introducing fluctuations, a rich collection of patterns emerge over time, in which spotted patterns migrate, combine, and replicate. In both of the applications, the adaptive features of the stochastic numerical methods are used to track at high resolution regions where the reactions are chemically active.

9.1. Modeling the chemical reactions

A number of modeling issues arise for the chemical reactions in the stochastic equations, which are not present in the deterministic setting. In the deterministic setting, it is usually assumed that the chemical species are locally well-mixed [74]. This allows at each point in space for reactions to be modeled at the mean-field level using the same expressions as for a homogeneous reaction chamber. In the stochastic setting the concentration field is no longer well-defined pointwise so alternatives must be developed.

A widely used approach is to regularize the concentration fields over the length scale of the discretization lattice. This is often done by using in the reaction expression the point-wise value from the discretized concentration field, which corresponds to the locally averaged concentration over a partition cell. This has the potential to cause issues in the convergence of the methods since the rate of reactions may depend sensitively on the numerical scheme and discretization parameters, such as the discrete lattice spacing [6,55,56,58–60]. For such methods, spatial discretization parameters often must be carefully tuned not to be too large or too small relative to the distance molecules migrate between chemical reactions (reaction mean-free path) to obtain physically reasonable results [6,55,56,58,74].

To avoid fine tuning of the discretization, we introduce additional parameters in our physical models which are independent of the discretization. The parameters are used in regularization procedures which average the stochastic concentration field to obtain values for use in reaction expressions. Many regularization procedures can be considered for the stochastic fields. Ideally, such a procedure would be based on studies of particle models, dynamic simulations, or analytic reductions of models to continuum descriptions, such as a Mori–Zwanzig theory [55,57,68,69,71,72,74–77]. Here, we take a more phenomenological approach.

To model the chemical reactions we use a functional of the following form

$$\mathbf{F}[c](\mathbf{x},t) = \int \alpha(\mathbf{x},\mathbf{y},\eta(\mathbf{y},t))d\mathbf{y}, \tag{9.1}$$

$$\eta(\mathbf{y},t) = \int \beta(\mathbf{y},\mathbf{z})c(\mathbf{z},t)d\mathbf{z}. \tag{9.2}$$

The α, β are assumed to be smooth functions which are compactly supported. The integration used to obtain η has the effect of smoothing the concentration field over a length scale ℓ, corresponding to the support of β. The term α uses these regularized concentration values and determines the rate at which the chemical reactions change the concentration of each molecular species.

The regularization of solutions of Eq. (2.2) for use in the functional $\mathbf{F}$ can be conceptually motivated by thinking about a collection of individual molecules which are distributed in space consistently with the continuum concentration field. The kernels are motivated conceptually by thinking about how the molecules diffusively migrate and react over time. The change in the spatial distribution of the molecules and in the type of the molecules ideally would yield the rates used for the change in the continuum concentration field. From this point of view, the α accounts for the rate at which molecules of each chemical species are introduced or removed at location $\mathbf{x}$ by the reactions. The β term models the fraction of molecules at location $\mathbf{z}$ which migrate to participate in chemical reactions associated with location $\mathbf{y}$. We discuss specific choices for the kernels in Eq. (9.2) in the context of applications in Sections 9.2 and 9.3.

9.2. Microorganism direction sensing using concentration gradients

The spatial distribution of chemical species plays a fundamental role in many processes in cell biology [1]. The bacterium *Escherichia coli* detects gradients in the concentration of important nutrients in the environment. The cell uses this information to move toward more nutrient rich regions. Individual *Dictyostelium discoideum* bacterium cells respond to spatial and temporal features of concentration fields of signaling molecules, such as cAMP generated by other cells, to coordinate collective movements which result in the formation of fruiting bodies and spores [39,40]. In the development of multicellular organisms, concentration fields of signaling molecules are used to determine cell differentiation and organization within tissues [1,43,73,83,84]. The study of the basic mechanisms by which cells detect local concentration gradients and respond is a fundamental part of cell biology.

Features of the external signaling concentration field are detected by cells through the binding of signaling molecules to receptor proteins which reside in the outer cell membrane. Upon binding, receptor proteins undergo conformational changes which trigger local chemical reactions which produce products which diffuse along the cell membrane or into the cytoplasm [1,83,84]. While many proteins and metabolites involved in these processes are known, there remain many questions about the particular interactions and mechanisms by which the external concentration field is detected and by which a cellular response is generated. Currently, this is an active area of experimental and theoretical research [44,78,80–82,84,86,87].

We investigate one mechanism recently proposed for the detection of concentration gradients [33]. We study the role played by fluctuations in the external concentration field of a signaling chemical species. To appreciate the possible importance of concentration fluctuations, it is illustrative to characterize the length and time scales encountered by individual cells. The signaling chemical species in the typical environment of a cell can have concentrations ranging from as small as a picomolar (pM) to as large as molar (M), see [1,35,85,86].

For illustrative purposes, we consider an intermediate concentration of 1mM and the length scale of a 100nm cubic box. One millimolar corresponds to $mM = 10^{-3} N_A/\text{litre} = 6.022 \times 10^{23}$ molecules/m^3, where N_A is Avogadro's number. On the length scale of 100 nm there is on average only 6.022×10^2 molecules per box. For a rough estimate of the time scale of the fluctuations we note that typical signaling molecules, such as cAMP, have diffusion coefficients on the order of 10^8 nm^2/s, see [29]. For a box with edge length $\ell = 100$ nm the amount of time required for a particle to diffuse out of the box is of the order $\tau_D = \ell^2/D = 10^{-4}$ s. This provides a rough estimate of the time scale on which fluctuations are expected to be correlated. For very shallow concentration gradients, cells are observed to change course in chemotaxis on the time scale of seconds or faster. This suggests that concentration fluctuations may play an important role [36]. We show how Eqs. (2.1)–(2.6) and (2.7) and the proposed numerical methods can be used to investigate the role of fluctuations in the concentration of the signaling chemical species.

To model how a cell initially processes a signal detected by membrane receptors, we consider a system of three basic chemical species which originate and diffuse within the cellular membrane. The chemical species are (i) an activator molecular species denoted by E, (ii) an inhibitor molecular species denoted by I, and (iii) a reporter molecular species denoted by Q. The reporter species Q is meant to account for how the receptor binding events result in an internal chemical signal which feeds into further cellular reactions. The internal chemical signal could take the form of chemical products within the cell membrane or cytoplasm. The internal chemical could signal cell motility through local activation of actin polymerization, cell polarization, or calcium release from local buffers/internal stores [1,12,33,41,84,86].

In our model, we consider each of the molecular species as being in one of two possible forms: active or inactive, which are denoted by P^* and P, respectively. Transitions between inactive and active can occur, for example, through phosphorylation or methylation of the individual proteins. We generically refer to this as the production of the active species or deactivation of the active species. In the model, we posit that the cell processes the external signal to form the reporter products Q by two competing processes. The first involves increases in the concentration of species E which increases the local

production of the active reporter species $Q^* \to Q$. The second involves increases in the concentration of species I which increases the local deactivation of the reporter species $Q \to Q^*$. The external concentration field influences these processes through the receptor binding events which locally produce active species of E and I. More precisely, the model for the chemical species inside the biological cell is given by the following system of reaction–diffusion equations

$$\frac{\partial E}{\partial t} = D_E \Delta E - \kappa_{de} E + \kappa_{re} S, \tag{9.3}$$

$$\frac{\partial I}{\partial t} = D_I \Delta I - \kappa_{di} I + \kappa_{ri} S, \tag{9.4}$$

$$\frac{\partial Q}{\partial t} = D_Q \Delta Q + \kappa_{qe} E (Q_T - Q) - \kappa_{qi} I Q. \tag{9.5}$$

The total concentration of the reporter species is denoted by $Q_T = Q^* + Q$. The S denotes the local concentration of the external signaling chemical species which is bound to membrane receptors. The biological cell is modeled spatially as a domain having the geometry of a disk of radius R. The cell membrane corresponds to the circle of radius R, see Fig. 9.1. The Eqs. 9.3, 9.4 and 9.5 should be considered to reside on this circular membrane with periodic boundary conditions. Three dimensional models can also be considered using an approach similar to what we present.

The external concentration field $c(\mathbf{x}, t)$ is obtained as the solution of

$$\frac{\partial c}{\partial t} = D_C \Delta c + \eta, \tag{9.6}$$

$$\langle \eta(\mathbf{x}, t) \eta(\mathbf{x}', t') \rangle = -2 D_C \Delta \delta(\mathbf{x} - \mathbf{x}') \delta(t - t'). \tag{9.7}$$

For the specific choice of diffusivity tensor $\mathbf{D} = D_C I$, this is Eq. (2.2). The concentration equation is solved on the domain exterior to the disk of radius R of the biological cell and between two walls of experimental apparatus which maintain a fixed level of concentration. To model no-flux of the signaling molecule into the biological cell, Neumann conditions are imposed on the boundary of the disk. To model the constant level of concentration maintained at each of the walls, Dirichlet conditions are imposed. The Dirichlet conditions are used to generate a concentration gradient by imposing different concentration levels at each of the walls. For the remaining top and bottom boundaries of the spatial domain, periodic boundary

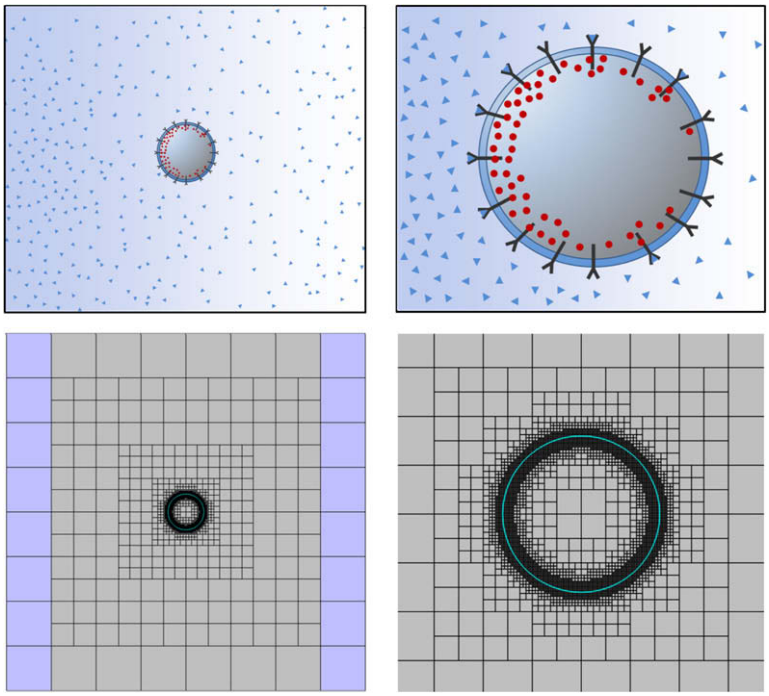

Fig. 9.1. Microorganism direction sensing based on concentration gradients: basic mechanism by which a single cells senses an environmental concentration gradient through receptor binding of an external chemical species (top left). Chemical signals are generated within the cell from bound receptors which indicate the direction of the gradient (top right). An adaptive multilevel mesh is used to spatially discretize the system on the domain exterior to the cell and between two walls of apparatus which control the concentration of external signaling molecules (lower left). The mesh is refined many levels near the surface of the cell to attain a high level of resolution and to capture well the geometry of the curved boundaries (lower right). Periodic boundary conditions are imposed on the upper and lower boundaries of the domain. Dirichlet boundary conditions are imposed on the left and right boundaries of the domain.

conditions are imposed. To capture the geometry of the domain for the solution we use a mesh which is both adaptive in space and includes cut-cells near the curved surface of the biological cell, see Fig. 9.1. More complex geometries in two and three dimensions can also be considered with a fairly straight-forward extension of the methodology proposed here.

An interesting feature of the model is the explicit representation of the external concentration field and its solution for the given geometry of the cell. In many models in the literature a linear gradient is imposed for use in the internal chemical kinetics of the cell. We find by solving the deterministic equations that the concentration gradient is in fact non-linear when taking into account the no-flux boundary conditions and cellular geometry. The geometry enhances at the cell surface the largest and smallest concentrations, which serves to amplify locally the concentration differences induced by the conditions at the walls. This often overlooked feature could have important implications for the behaviors of models used for interpreting experimental data.

The external concentration field influences the production rates of internal chemical species by receptor binding events. The receptor binding events are modeled at a coarse level by considering the local number of molecules which are in the vicinity of a receptor cluster. In the model we use a finite number of receptor clusters indexed by i and located at $\mathbf{x}_i$. The number of molecules n_i in the vicinity of the ith cluster is obtain from the external concentration field by

$$n_i = \int \Lambda(|\mathbf{x} - \mathbf{x}_i|) c(\mathbf{x}, t) d\mathbf{x}. \tag{9.8}$$

The kernel is defined by $\Lambda(r) = 1$ for $r < a$ and zero otherwise. For the number of molecules bound to the ith receptor cluster, we use the number density field

$$S_i(\mathbf{x}, t) = \alpha n_i \delta(\mathbf{x} - \mathbf{x}_i). \tag{9.9}$$

The parameter α accounts for the fraction of molecules in the vicinity of the cluster which are bound to a receptor. For the concentration field of all signaling molecules bound to the receptors, we use

$$S(\mathbf{x}, t) = \sum_i S_i(\mathbf{x}, t). \tag{9.10}$$

This concentration field S plays an important role in the model by activating the excitatory chemical species at the rate $\kappa_{re}S$ and activating the inhibitory chemical species at rate $\kappa_{ri}S$, see Eq. (9.3).

We investigate the effect of fluctuations on the cells ability to detect an external concentration gradient. We consider the case where the external concentration gradient is small relative to the magnitude of the relevant fluctuations. To parameterize appropriately the model for this physical regime, we use kinetic rates and diffusion coefficients on the same order of magnitude as rates found in the experimental and theoretical cell biology literature [28–37]. A summary of our specific choice of parameters can be found in Tables 9.1 and 9.2.

The external signaling molecules are taken to have diffusion coefficients on the order of 10^8 nm^2 s^{-1}. This choice was made since the signaling molecule cAMP is reported to have a diffusion coefficient of $2.7 \pm 0.2 10^8$ nm^2 s^{-1}, see [29]. We use diffusion coefficients for molecules diffusing inside of the cell in the reported range 10^5 nm^2 s^{-1}—10^7 nm^2 s^{-1}, see [30,31]. Concerning the overall time scales associated with cell gradient sensing, it is observed that cells are able to respond to changes in the external concentration field on the order of seconds [33,39]. The rates of the first order rates in the biochemical chemical reactions are taken to range from 1 s^{-1} to 10^4 s^{-1}. The rates of the second order rates in the biochemical chemical reactions are taken to range from10^{-1} mM^{-1} s^{-1} to 1 mM^{-1}s^{-1}.

Simulations of the cell gradient sensing mechanism were carried out by using the introduced stochastic numerical methods. A time step of 2.5×10^{-5} s was used and the model was simulated for 1.6×10^6 time steps corresponding to a physical time scale of 40 s. For the proposed gradient sensing mechanism, it was found that directions can be reliably detected even when subject to significant concentration fluctuations in the external signaling chemical species. The robustness of the basic

Table 9.1
Cell gradient sensing model: description of the parameters.

Parameter	Description
R	radius of the disk-shaped cell
D_C	diffusion coefficient of external signaling chemical species
a	receptor sensor associated length scale
D_E	diffusion coefficient of excitatory chemical species
κ_{re}	rate of receptor initiated activation of excitatory chemical species
κ_{de}	rate of degradation/deactivation of excitatory chemical species
D_I	diffusion coefficient of inhibitory chemical species
κ_{ri}	rate of receptor initiated activation of inhibitory chemical species
κ_{di}	rate of degradation/deactivation of inhibitory chemical species
Q_T	total concentration of reporter chemical species
D_Q	diffusion coefficient of reporter chemical species
κ_{qe}	rate of production of active reporter aided by the excitatory chemical species
κ_{qi}	rate of degradation/deactivation of active reporter aided by the inhibitory chemical species

Table 9.2
Cell gradient sensing model: values of the parameters.

Parameter	Description
R	2×10^4 nm
D_C	10^8 nm^2 s^{-1}
a	100 nm
D_E	10^6 nm^2 s^{-1}
κ_{re}	10^4 s^{-1}
κ_{de}	10^4 s^{-1}
D_I	5×10^7 nm^2 s^{-1}
κ_{ri}	1 s^{-1}
κ_{di}	1 s^{-1}
Q_T	100 mM
D_Q	10^6 nm^2 s^{-1}
κ_{qe}	10^{-1} mM^{-1} s^{-1}
κ_{qi}	1 mM^{-1} s^{-1}

mechanism hinges on the reporter chemical species reaching a steady-state concentration on times scales long relative to the correlation time scale of the fluctuations. The slow response of the inhibitor and reporter act to filter out many of the fluctuations of the external concentration field. This has the effect of yielding a mean signal which reliably indicates the direction of the gradient. The simulation results for the fluctuations of the signaling and intracellular chemical species are reported in Fig. 9.2.

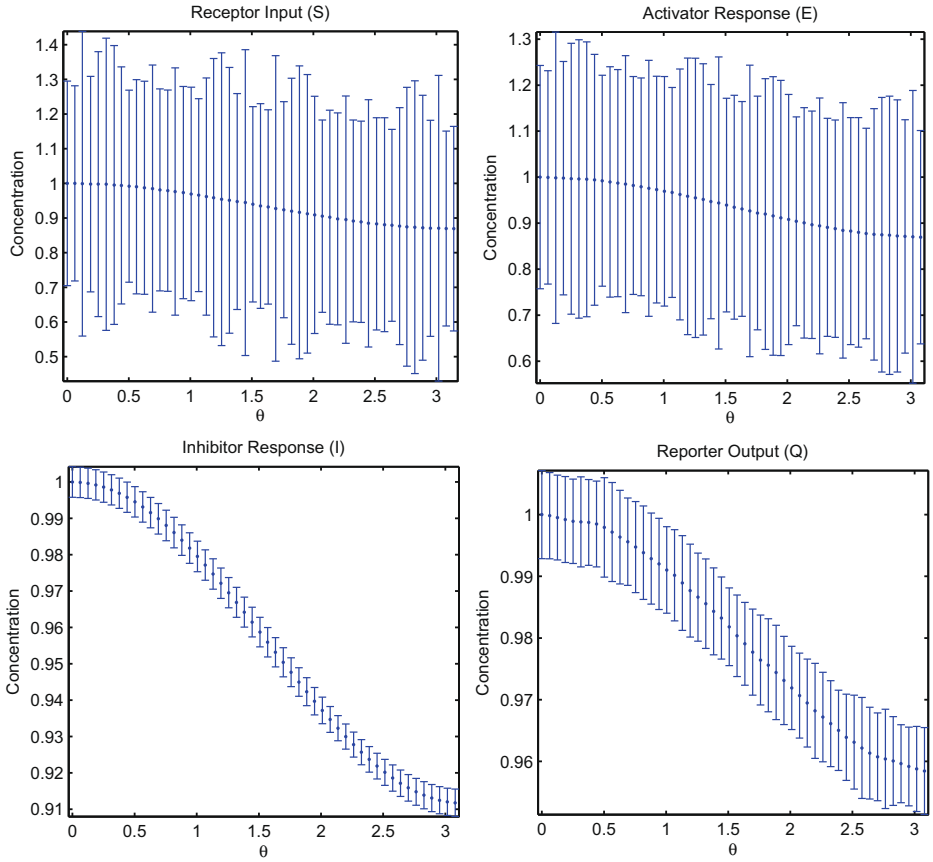

Fig. 9.2. Simulation results for the gradient sensing model. The mean concentration fields are plotted by the symbol · along with estimated error bars corresponding to three standard deviations. For clarity, the concentration levels are scaled by the maximum mean concentration value for each chemical species. The receptor activation level has a shallow concentration gradient obscured by fluctuations, see upper left. This had maximum mean concentration of 1.5 mM. The inhibitor responds slowly to external signals and acts to filter out fluctuations, see bottom left. This had maximum mean concentration of 1.5 mM. The activator chemical species responds quickly to external signals and exhibits significant fluctuations, see bottom right. This had maximum mean concentration of 1.5 mM. The concentration profile of the reporter chemical species which diffuses in the cell membrane yields a robust signal, see top right. The maximum mean concentration was 9.3 mM. The combination of slow inhibitor and fast activator acts to yield a filtered signal which robustly indicates the gradient direction.

9.3. Fluctuation induced pattern formation in spatially extended systems

Spatial patterns emerge in many deterministic reaction–diffusion systems. A widely studied mechanism is the Turing instability. In the Turing instability, the diffusion of the chemical species act in concert with the chemical reactions to destabilize the spatially homogeneous steady-state [49]. In the deterministic case of only two chemical species, the Turing instability requires the reactions to include both positive and negative feedback in the rates of production of the chemical species [51,52]. We consider a related mechanism by which patterns can be induced in spatially extended systems. Instead of the mean diffusive concentration flux acting alone with the reactions to induce the formation of patterns, we discuss a parameter regime in which the fluctuations serve to destabilize a linearly stable steady-state. We consider parameters for which the deterministic system settles into a stable steady-state while the stochastic system exhibits a rich collection of spatial patterns which continually grows over time.

We consider a reaction–diffusion system with chemical reactions which are a variant of the Gray–Scott reactions [64,65]. Using Eq. (2.2), the reaction–diffusion equations can be expressed as

$$\frac{\partial u}{\partial t} = D_1 \Delta u + f[u, v] + \eta_1, \tag{9.11}$$

$$\frac{\partial v}{\partial t} = D_2 \Delta v + g[u, v] + \eta_2, \tag{9.12}$$

where η_1, η_2 account for the concentration fluctuations and are Gaussian random fields with mean zero and covariance

$$\langle \eta_1(\mathbf{x}, t)\eta_1(\mathbf{x}', t')\rangle = -2\bar{u}D_1\Delta_{\mathbf{x}}\delta(\mathbf{x}-\mathbf{x}')\delta(t-t'), \tag{9.13}$$

$$\langle \eta_2(\mathbf{x}, t)\eta_2(\mathbf{x}', t')\rangle = -2\bar{v}D_2\Delta_{\mathbf{x}}\delta(\mathbf{x}-\mathbf{x}')\delta(t-t') \tag{9.14}$$

$$\langle \eta_1(\mathbf{x}, t)\eta_2(\mathbf{x}', t')\rangle = 0. \tag{9.15}$$

This corresponds to the choice of the diffusion tensor with block diagonal matrices $D_1 I$ and $D_2 I$ in Eq. (2.2). The I denotes the identity matrix. The D_1, D_2 denote the scalar isotropic diffusion coefficients of the chemical species. The chemical reactions of the molecular species are accounted for by the functionals f, g. In the reaction–diffusion system the concentrations of the chemical species are chosen to be nearly homogeneous with only small variations in space. For this purpose, we use a variant of the Gray–Scott reactions which we express as cubics of the form

$$f[u, v](\mathbf{x}, t) = \alpha_6 n_u n_v^2 + \alpha_5 n_u^2 + \alpha_4 n_v^2 + \alpha_3 n_u n_v + \alpha_2 n_u + \alpha_1 n_v + \alpha_0, \tag{9.16}$$

$$g[u, v](\mathbf{x}, t) = \beta_6 n_u n_v^2 + \beta_5 n_u^2 + \beta_4 n_v^2 + \beta_3 n_u n_v + \beta_2 n_u + \beta_1 n_v + \beta_0. \tag{9.17}$$

To determine the local number of molecules which participate in reactions, we use a regularization of the form discussed in Section 9.1

$$n_u(\mathbf{x}, t) = \int \Lambda(\mathbf{y}-\mathbf{x})u(\mathbf{y}, t)d\mathbf{y}, \tag{9.18}$$

$$n_v(\mathbf{x}, t) = \int \Lambda(\mathbf{y}-\mathbf{x})v(\mathbf{y}, t)d\mathbf{y}. \tag{9.19}$$

The kernel is $\Lambda(\mathbf{z}) = (1/2\pi\sigma^2)\exp(-|\mathbf{z}|^2/2\sigma^2)$. This provides a regularization of the concentration field over the length scale σ for use in the reactions expressions. To obtain a discrete approximation on the multilevel mesh to the integrals in Eqs. (9.18) and (9.19), we use

$$\tilde{n}_{u,\mathbf{m}} = \sum_{\mathbf{m}} \tilde{\Lambda}_{\mathbf{m},\mathbf{n}} c_{\mathbf{m}} \Delta y_{\mathbf{m}}, \tag{9.20}$$

$$\tilde{\Lambda}_{\mathbf{m},\mathbf{n}} = \frac{1}{Z_{\mathbf{m}}}\Lambda(\mathbf{x}_{\mathbf{m}}-\mathbf{x}_{\mathbf{n}})\Delta x_{\mathbf{n}}^d, \tag{9.21}$$

$$Z_{\mathbf{m}} = \sum_{\mathbf{n}} \Lambda(\mathbf{x}_{\mathbf{m}}-\mathbf{x}_{\mathbf{n}})\Delta x_{\mathbf{n}}^d. \tag{9.22}$$

We use a similar definition for $\tilde{n}_{v,\mathbf{m}}$. The $Z_{\mathbf{m}}$ normalizes the discretized kernel so the sum of the kernel over the mesh evaluates to one. As the mesh is refined $\Delta x \to 0$, it follows that $Z_{\mathbf{m}} \to 1, \tilde{n}_{u,\mathbf{m}} \to n_u$, and $\tilde{n}_{v,\mathbf{m}} \to n_v$. This ensures as the mesh is refined a well-defined limit is obtained for the reaction expressions.

To study the model in a regime in which the concentrations of the chemical species are nearly homogeneous and exhibit interesting dynamics we use the parameter values in Table 9.3. For the chemical reactions there is an associated non-spatial two dimensional dynamical system defined by f, g. The phase portrait of this dynamical system is given in Fig. 9.3. For the choice of parameters, the system has dynamics in which there is only one stable steady-state at $n_u = 1.1,\ n_v = 1.0$.

To study a possible mechanism by which fluctuations can induce patterns, we choose parameters so that the phase space exhibits some special features. In the phase space there is a region in which two nullclines pass in close proximity. This indicates the chosen parameters are close to a bifurcation [88]. Given this proximity of the nullclines, even relatively small perturbations to the dynamical system can cause a crossing of the nullclines. Such back and fourth switching has the potential to destabilize the steady-state, which is the mechanism we consider, see Fig. 9.3.

Table 9.3
Reaction–diffusion system: values of the parameters.

Parameter	Description
$[\alpha_0, \alpha_1, \alpha_2, \alpha_3, \alpha_4, \alpha_5, \alpha_6]$	$[1.100605, -2.2, -1.10055, 2.2, 1.1, 0.0, -1.1] \times 10^6$
$[\beta_0, \beta_1, \beta_2, \beta_3, \beta_4, \beta_5, \beta_6]$	$[-0.998845, 1.998845, 1.0, -2.0, -1.0, 0.0, 1.0] \times 10^6$
D_u	5.5×10^3
D_v	5.0×10^3
L	5.632×10^2
$\bar{u}$	1.1
$\bar{v}$	1.0

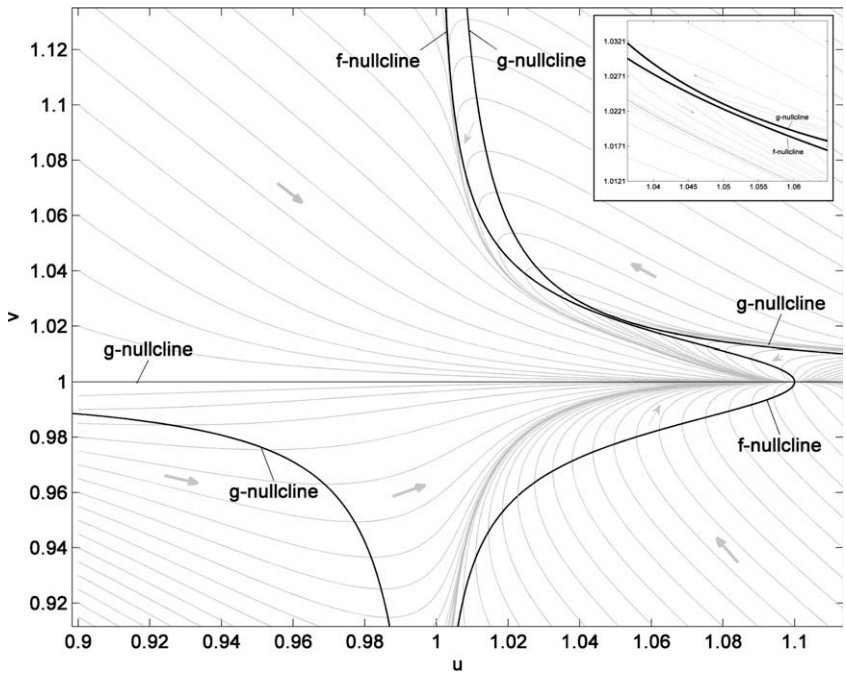

Fig. 9.3. Phase portrait of the local dynamics associated with the chemical reactions. There is one stable steady-state at $u = 1.1,\ v = 1.0$. Shown in the inset is the region of phase space where the nullclines pass in close proximity, $1.03 < u < 1.07$.

In the reaction–diffusion system, the dynamical system associated with the chemical reactions can be associated with the local dynamics of the system. The diffusion of chemical species acts to couple laterally these local dynamical systems. Perturbations are introduced in the local dynamics through the concentration fluctuations. To investigate the behavior of the reaction–diffusion system when subject to fluctuations, we use the developed stochastic numerical methods to approximate Eq. (9.12). To track regions in which the chemical reactions are most active, an adaptive mesh is introduced which refines the mesh for any concentration of v above a critical threshold.

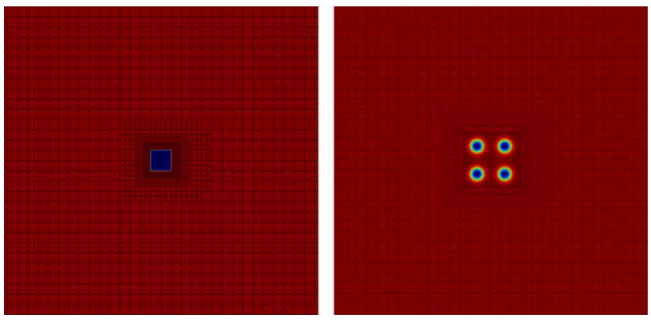

Fig. 9.4. Reaction–diffusion system in the deterministic case.

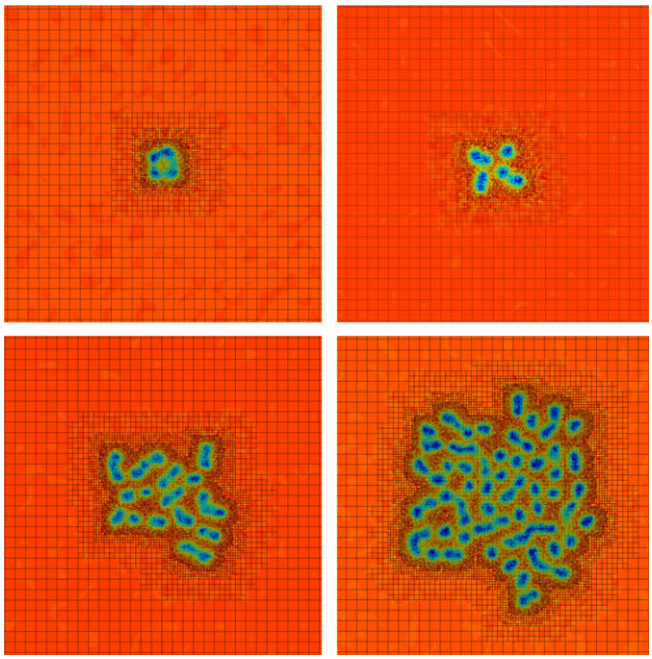

Fig. 9.5. Reaction–diffusion system with concentration fluctuations. The fluctuations induce a rich spatial pattern of spots which replicate, migrate, and merge. Shown is the concentration field of u for the time steps $10^3,\ 10^4,\ 4\times10^4,\ 7\times10^4$, where $\Delta t = 0.1$. It is found that the spatial patterns grow to fill the entire domain. Periodic boundary conditions are imposed at the domain boundaries. For refinement, a threshold is set for the concentration of v in a localize region. The refinement is triggered when v is found above the threshold.

In the simulations an initial perturbation is introduced into the system in which a small square region centered at the origin of edge length 17.6 is set to $u = 1.07,\ v = 1.03$. The concentrations are set elsewhere to be $u = 1.1,\ v = 1.0$. This initial perturbation is introduced to avoid having to simulate fluctuations over a potentially long period of time to observe a "nucleating event", which breaks sufficiently the translational symmetry of the homogeneous state. While spontaneous realization of configurations similar to the initial perturbation are likely rare, they do have a non-zero probability of occurring in the fluctuating stochastic system. To ensure the initial perturbation alone is not responsible for the observed results, simulations were performed in the absence of fluctuations. For the deterministic system, it was found that a simple symmetric pattern of only four spots is obtained and appears to be stable, see Fig. 9.4.

To investigate the reaction–diffusion system with fluctuations, simulations were performed using the developed stochastic numerical methods. Using the same initial conditions as in the deterministic case, it is found that a rich collection of patterns emerge. The pattern takes the form of spots which continually grow, migrate and replicate, see Fig. 9.5. Movies of the full evolution process of the emerging pattern can be found on-line [79]. The simulation results show that fluctuations have the potential to induce the formation of interesting patterns in spatially extended systems.

10. Conclusions

Stochastic Partial Differential Equations (SPDEs) were introduced for modeling concentration fluctuations in reaction diffusion-systems. The SPDEs account for fluctuations arising primarily from the finite number of molecules which undergo diffusive migrations as opposed to arising from the chemical reactions. For numerical approximation of the non-classical solutions of the SPDEs a discretization approach was introduced. The discretizations for the stochastic driving fields were derived by controlling errors in how the equilibrium fluctuations of the discrete system approximate those of the continuum system. For the discretized stochastic driving fields, algorithms were developed for the efficient generation of random variates with the required covariance structure. Stochastic numerical methods were developed and demonstrated for discretizations on meshes with multiple levels of resolution and on domains having curved boundaries. The approaches introduced for the derivation of discretizations for the SPDEs and for the development of the stochastic numerical methods are expected to be widely applicable in the study of spatially extended stochastic systems.

Acknowledgments

The author would like to acknowledge support from the research grant NSF DMS-0635535. The author would like to thank Alexander Roma and Boyce Griffith for helpful suggestions concerning adaptive numerical methods. The author would

also like to thank Samuel Isaacson for stimulating discussion concerning reaction–diffusion systems. The work on microorganism gradient sensing benefited from talks and discussion at the May 2008 workshop *Quantitative Approaches to Cell Motility* at the Institute for Mathematics and its Applications (IMA) at the University of Minnesota.

Appendix A. Supplementary material

Supplementary data associated with this article can be found, in the online version, at doi:10.1016/j.jcp.2010.01.012.

References

[1] B. Alberts, A. Johnson, J. Lewis, M. Raff, K. Roberts, P. Walker, Molecular Biology of the Cell, Garland Publishing, 2002.
[2] L.E. Reichl, A Modern Course in Statistical Physics, second ed., John Wiley & Sons Inc., New York, 1998.
[3] D. Frenkel, B. Smit, Understanding Molecular Simulation, second ed., Academic Press, 2002.
[4] H. Ruben, Generalised concentration fluctuations under diffusion equilibrium, J. Appl. Prob. 1 (1964) 7–68.
[5] R.F. Fox, G.E. Uhlenbeck, Contributions to non-equilibrium thermodynamics: I. Theory of hydrodynamic fluctuations, Phys. Fluid 13 (1970) 8.
[6] F. Baras, M.M. Mansour, Reaction–diffusion master equation: a comparison with microscopic simulations, Phys. Rev. E 54 (6) (1996).
[7] L.D. Landau, E.M. Lifshitz, Course of theoretical physics, Statistical Physics, vol. 9, Pergamon Press, Oxford, 1980.
[8] C.W. Gardiner, Handbook of Stochastic Methods: for Physics, Chemistry, and the Natural Siences Springer Series in Synergetics, second ed., Springer-Verlag, Berlin Heidelberg, New York, 1997.
[9] N.G. van Kampen, Stochastic Processes in Physics and Chemistry, North-Holland Publishing, 1981.
[10] P.E. Kloeden, E. Platen, Numerical Solution of Stochastic Differential Equations, Springer-Verlag, 1992.
[11] B. Oksendal, Stochastic Differential Equations: An Introduction with Applications, Springer, 2000.
[12] G. Oster, A. Mogilner, Force generation by cellular polymers, in: A. Ciferri (Ed.), Supramolecular Polymers, second ed., CRC Press, 2005, pp. 741–752.
[13] P.J. Atzberger, P.R. Kramer, C.S. Peskin, A stochastic immersed boundary method for fluid–structure interactions at microscopic length scales, J. Comput. Phys. 224 (2) (2007).
[14] B.E. Griffith, Simulating the Blood-muscle-valve Mechanics of the Heart by an Adaptive and Parallel Version of the Immersed Boundary Method, Ph.D. Thesis, Courant Institute of Mathematical Sciences, New York University, 2005.
[15] A.M. Roma, A Multilevel Self Adaptive Version of the Immersed Boundary Method., Ph.D. Thesis, Courant Institute of Mathematical Sciences, New York University, 1996.
[16] M.L. Minion, A projection method for locally refined grids, J. Comput. Phys. 127 (1) (1996) 158–178.
[17] P. McCorquodale, P. Collela, H. Johansen, A Cartesian grid embedded boundary method for the heat equation on irregular domains, J. Comput. Phys. 173 (2001) 620–635.
[18] T. Ye, R. Mittal, H.S. Udaykumar, W. Shyy, An accurate cartesian grid method for viscous incompressible flows with complex immersed boundaries, J. Comput. Phys. 156 (1999) 209–240.
[19] J.J. Quirk, An alternative to unstructured grids for computing gas dynamic flows around arbitrarily complex two-dimensional bodies, Comput. Fluids 23 (I) (1994) 125–142.
[20] M. Berger, M. Aftosmis, J. Melton, Accuracy, adaptive methods and complex geometry, in: L. Sakell, D. Knight (Eds.), Proceedings of First AFOSR Conference on Dynamic Motion CFD Rutgers University, June 1996.
[21] D.M. Ingram, D .M. Causon, C.G. Mingham, Developments in Cartesian cut cell methods, Math. Comput. Simulat. 61 (2003) 561–572.
[22] W.J. Coirier, K.G. Powell, An accuracy assessment of Cartesian-mesh approaches for the Euler equations, J. Comput. Phys. 117 (1995) 121–131.
[23] M.S. Day, P. Colella, M.J. Lijewski, C.A. Rendleman, D.L. Marcus, Embedded Boundary Algorithms for Solving the Poisson Equation on Complex Domains, Lawrence Berkeley National Laboratory, Paper LBNL-41811, %3chttp://repositories.cdlib.org/lbnl/LBNL-41811%3e, 1998.
[24] E.W. Cheney, Introduction to Approximation Theory, American Mathematical Society, 1982.
[25] J.P. Boyd, Chebyshev and Fourier Spectram Methods, Dover Publications, New York, 2001.
[26] A. Keese, A Review of Recent Developments in the Numerical Solution of Stochastic Partial Differential Equations (Stochastic Finite Elements), Thesis, Institute of Scientific Computing, Technical University Braunschweig, Brunswick, Germany, 2003.
[27] F.E. Benth, J. Gjerde, Convergence rates for finite element approximations for stochastic partial differential equations, Int. J. Probability Stochastic Process. 63 (1998) 313–326.
[28] M. Postma, P.J.M. Van Haastert, A diffusion/translocation model for gradient sensing by chemotactic cells, Biophys. J. 81 (2001) 1314–1323.
[29] C. Chen, T. Nakamura, Y. Koutalos, Cyclic AMP diffusion coefficient in frog olfactory cilia, Biophys. J. 76 (1999) 2861–2867.
[30] H. Niv, O. Gutman, Y.I. Henis, Y. Kloog, Membrane interactions of a constitutively active GFP-Ki-Ras 4B and their role in signaling. Evidence from lateral mobility studies, J. Biol. Chem. 274 (1999) 1606–1613.
[31] M. Arrio-Dupont, G. Foucault, M. Vacher, P.F. Devaux, S. Cribier, Translational diffusion of globular proteins in the cytoplasm of cultured muscle cells, Biophys. J. 78 (2000) 901–907.
[32] J. Krishnan, P.A. Iglesias, Analysis of the signal transduction properties of a module of spatial sensing in eukaryotic chemotaxis, Bull. Math. Biol. 65 (2003) 95–128.
[33] P.A. Iglesias, P.N. Devreotes, Navigating through models of chemotaxis, Curr. Opin. Cell Biol. 20 (2008) 35–40.
[34] M.I. Monine, A.M. Berezhkovskii, E.J. Joslin, H.S. Wiley, D.A. Lauffenburger, S.Y. Shvartsman, Ligand accumulation in autocrine cell cultures, Biophys. J. 88 (2005) 2384–2390.
[35] D. Ishii, K.L. Ishikawa, T. Fujita, M. Nakazawa, Stochastic modelling for gradient sensing by chemotactic cell, Sci. Technol. Adv. Mater. 5 (2004) 715–718.
[36] H.C. Berg, E.M. Purcell, Physics of chemoreception, Biophys. J. 20 (1977).
[37] A. Narang, K.K. Subramanian, D.L. Lauffenburger, A mathematical model for chemoattractant gradient sensing based on receptor-regulated membrane phospholipid signaling dynamics, Ann. Biomed. Eng. 29 (2001) 677–691.
[38] M.D. Onsum, K. Wong, P. Herzmark, H.R. Bourne, A.P. Arkin, Morphology matters in immune cell chemotaxis: membrane asymmetry affects amplification, Phys. Biol. 3 (2006) 190–199.
[39] C.L. Manahan, P.A. Iglesias, Y. Long, P.N. Devreotes, Chemoattractant signaling in *Dictostelium discoideum*, Annu. Rev. Cell Dev. Biol. 20 (2004) 223–253.
[40] H. Zhang, M. ?R. Gomez-Garcia, M.R.W. Brown, A. Kornberg, Inorganic polyphosphate in *Dictyostelium discoideum*: influence on development, sporulation, and predation, PNAS 102 (8) (2005) 2731–2735.
[41] M. Onsum, C.V. Rao, A mathematical model for neutrophil gradient sensing and polarization, PLoS Comput. Biol. 3 (3) (2007).
[42] H. Royden, Real Analysis, Simon & Schuster Company, 1988.
[43] T.M. Keenan, A. Folch, Biomolecular gradients in cell culture systems, Royal Soc. Chem. Lab. Chip 8 (2008) 34–57.
[44] N. Andrew, R.H. Insall, Chemotaxis in shallow gradients is mediated independently of PtdIns 3-kinase by biased choices between random protrusions, Nature Cell Biol. 9 (2) (2007).
[45] G. Da Prato, J. Zabczyk, Stochastic Equations in Infinite Dimensions, Cambridge University Press, 1992.
[46] E.H. Lieb, M. Loss, Analysis, American Mathematical Society, 1997.
[47] H. Holden, B. Oksendal, J. Uboe, T. Zhang, Stochastic Partial Differential Equations: A Modeling, White Noise Functional Approach, Birkhauser, 1996.

[48] H. Kunita, Generalized solutions of a stochastic partial differential equation, J. Theor. Probability 7 (2) (1994).
[49] A.M. Turing, The chemical basis of morphogenesis, Philos. Trans. R. Soc. London B 237 (1952) 37–72.
[50] W.C. Carter, J.E. Taylor, J.W. Cahn, Variational methods for microstructural-evolution theories, JOM of the The Minerals, Metals & Materials Society (TMS), 1997.
[51] J.D. Murray, Mathematical Biology, 2nd Corrected ed., Springer, 1993.
[52] J. Keener, J. Sneyd, Mathematical Physiology, Springer-Verlag, 1993.
[53] M. Mimura, Reaction–diffusion systems arising in biological and chemical systems: application of singular limit procedures, in: L. Ambrosio, K. Deckelnick, G. Dziuk, M. Mimura, V. Solonnikov, H.M. Soner (Eds.), Mathematical Aspects of Evolving Interfaces, Springer-Verlag, 2000.
[54] L.C. Evans, Partial Differential Equations, American Mathematical Society, 1998.
[55] S.A. Isaacson, C.S. Peskin, Incorporating diffusion in complex geometries into stochastic chemical kinetics simulations, SIAM J. Sci. Comput. 28 (1) (2006) 47–74.
[56] S.A. Isaacson, The reaction–diffusion master equation as an asumptotic approximation of diffusion to a small target, preprint, 2008.
[57] S.A. Isaacson, Relationship between the reaction? Diffusion master equation and particle tracking models, J. Phys. A 41 (2008) 065003.
[58] J. Elf, A. Doncic, M. Ehrenberg, Mesoscopic reaction–diffusion in intracellular signaling, Proc. SPIE 5110 (2003).
[59] F. Lesmes, D. Hochberg, F. Mora, J. Perez-Mercader, Noise-controlled self-replicating patterns, Phys. Rev. Lett. 91 (23) (2003).
[60] A. Munteanu, R.V. Sole', Pattern formation in noisy self-replicating spots, Int. J. Bifurcations Chaos 16 (12) (2006) 3679–3685.
[61] G. Strang, Linear Algebra and Its Applications, Harcourt Brace and Company.
[62] M. Hirsh, S. Smale, Differential Equations, Dynamical Systems, and Linear Algebra, Academic Press, New York, 1974.
[63] W.H. Press, Saul A. Teukolsky, W.T. Vetterling, B.P. Flannery, Numerical Recipes, Cambridge University Press, 2002.
[64] P. Gray, S.K. Scott, Sustained oscillations and other exotic patterns of behavior in isothermal reactions, J. Phys. Chem. 89 (1985) 22–32.
[65] K. Lee, W.D. McCormick, J.E. Pearson, H.L. Swinney, Experimental observation of self-replicating spots in a reaction–diffusion system, Nature 369 (1994).
[66] J. Stewart, Calculus, Thomson Brooks/Cole, 2009.
[67] L.N. Trefethen, D. Bau, Numerical Linear Algebra, Society of Industrial and Applied Mathematics, 1997.
[68] G.A. Bird, Molecular Gas Dynamics and the Direct Simulation of Gas Flows, Clarendon, Oxford, 1994.
[69] D.A. McQuarrie, Stochastoc approach to chemical kinetics, J. Appl. Prob. 4 (1967) 413–478.
[70] T. Leppanen, M. Karttunen, R.A. Barrio, K. Kaski, Turing systems as models of complex pattern formation, Brazilian J. Phys. 34 (2) (2004) 368–372.
[71] S.S. Andrews, D. Bray, Stochastic simulation of chemical reactions with spatial resolution and single molecule detail, Phys. Biol. 1 (2004) 137–151.
[72] F. Zaera, I. Rusinek, Monte Carlo simulation for inhomogeneous chemical kinetics: application to the Belousov–Zhabotinskii reaction, J. Comput. Chem. 2 (4) (1981) 402–409.
[73] T. Tabata, Y. Takei, Morphogens, their identification and regulation, Development 131 (2004) 703–712.
[74] D. Gillespie, A rigorous derivation of the chemical master equation, Phys. A 188 (1992) 404–425.
[75] K. Takahashi, S.N. Arjunan, M. Tomita, Space in systems biology of signaling pathways ? Towards intracellular molecular crowding in silico, FEBS Lett. 579 (2005) 1783–1788.
[76] A.J. Chorin, O.H. Hald, R. Kupferman, Optimal prediction and the Mori–Zwanzig representation of irreversible processes, PNAS 97 (7) (2000).
[77] D. Hochberga, M.P. Zorzano, F. Moran, Spatiotemporal patterns driven by autocatalytic internal reaction noise, J. Chem. Phys. 122 (2005) 214701.
[78] S. Funamoto, R. Meili, S. Lee, L. Parry, R.A. Firtel, Spatial and temporal regulation of 3-phosphoinositides by PI 3-Kinase and PTEN mediates chemotaxis, Cell 109 (2002) 611–623.
[79] P.J. Atzberger, <http://www.math.ucsb.edu/~atzberg/index.html>.
[80] C. Bouzigues, M. Morel, A. Triller, M. Dahan, Asymmetric redistribution of GABA receptors during GABA gradient sensing by nerve growth cones analyzed by single quantum dot imaging, PNAS 104 (27) (2007) 11251–11256.
[81] C.Y. Chung, S. Funamoto, R.A. Firtel, Signaling pathways controlling cell polarity and chemotaxis, TRENDS Biochem. Sci. 26 (9) (2001).
[82] N. Andrew, R.H. Insall, Chemotaxis in shallow gradients is mediated independently of PtdIns 3-kinase by biased choices between random protrusions, Nature Cell Biol. 9 (2) (2007).
[83] B. Shilo, N. Barkai, EGF receptor signaling? A quantitative view, Curr. Biol. 17 (24) (2007).
[84] S.Y. Shvartsman, H.S. Wiley, D.A. Lauffenburger, Epidermal growth factor receptor signaling in tissues, IEEE Control Syst. Mag. (2004).
[85] M.I. Monine, A.M. Berezhkovskii, et al., Ligand accumulation in autocrine cell cultures, Biophys. J. 88 (2005) 2384–2390.
[86] I.I. Moraru, L.M. Loew, Intracellular signaling: spatial and temporal control, Physiology 20 (2005) 169–179.
[87] T.M. Keenan, A. Folch, Biomolecular gradients in cell culture systems, Lab on a Chip 8 (2008) 34–57.
[88] J. Guckenheimer, P. Holmes, Nonlinear Oscillations, Dynamical Systems, and Bifurcations of Vector Fields, Springer-Verlag, New York, 1983.